STUDY ON LONG-RANGE SURFACE PLASMON RESONANCE BIOSENSOR USING ELECTROSPUN POLYMER FIBERS

PAPHAWADEE NETSUWAN

DOCTORAL PROGRAM IN ELECTRICAL AND INFORMATION ENGINEERING

GRADUATE SCHOOL OF SCIENCE AND TECHNOLOGY

NIIGATA UNIVERSITY

ACKNOWLEDGEMENT

I would like to express my sincere gratitude and appreciation to many people. First of all, I would like to thank my major research advisor, Assoc. Prof. Dr. Akira Baba and Asst. Prof. Dr. Saengrawee Sriwichai for their constant support in every aspect of my academic, their kind supervision, helpful guidance, corrections and support throughout the course of this research project.

I would also like to thank, Prof. Dr. Kazunai Shinbo, Prof. Dr. Keizo Kato and Prof. Dr. Futao Kaneko at Center for Transdisciplinary Research, Niigata University for their supports, inputs, knowledges and grateful kindness throughout my stay in Niigata University, Niigata, Japan, for their help, advice and useful suggestions during doing a research in Japan.

Special thanks to the Global Circus Program from Graduate School of Science and Technology Niigata University, the Commission on Higher Education, Ministry of Education, Rajamangala University of Technology Lanna and the Graduate School, Chiang Mai University, Thailand, for financial support throughout my study.

I would like to thanks all members of Center of Transdisciplinary Research, Niigata University, Japan and the Nanoscience Research Laboratory, Faculty of Chemistry, Chiang Mai University, Thailand, for their helpful, friendship and sharing many experiences in the laboratory providing the family type of feeling which is warm

and comfortable. I am also appreciated to helps and friendship from Hiroto Mimiya, Chutiparn Letvachirapaiboon, Rapiphun Janmanee, Sopis Chuekachang.

Finally, I would like to express my grateful and the deepest appreciation to all my family members.

Paphawadee Netsuwan

ABSTRACT

The fabrication of long-range surface plasmon resonance (LR-SPR) immunosensor from water-stable electrospun polyacrylic acid (PAA) fibers was studied. LR-SPR setup consists of thin gold film and layer of Cytop which let it has larger evanescent field intensity and penetration depth. The water-stable electrospun PAA fibers produced by adding β-cyclodextrin as crosslinker followed by thermal treatment at 180 °C for 40 min were fabricated onto the LR-SPR sensor surface. The free carboxyl group of electrospun PAA fibers was activated to immobilize antibody-antigen in immunosensor application. The layer-by-layer (LbL) system on the electrospun PAA fibers was performed to further increase water-stability of fibers and number of active carboxyl group. Therefore, the LR-SPR immunosensor based on water-stable electrospun PAA fibers was used to detect of human immunoglobulin G (IgG).

CONTENTS

CONTENTS (CONTINUED)

LIST OF TABLES

LIST OF FIGURES

LIST OF FIGURES (CONTINUED)

LIST OF FIGURES (CONTINUED)

LIST OF ABBREVIATIONS and SYMBOLS

ATR	Attenuated total internal reflection
A-IgG	Anti-human immunoglobulin G (Fab specific)
CD	Cyclodextrin
CPWR	Coupled plasmon waveguide resonance
EA-HCl	Ethanolamine hydrochloride
EDC	1-ethyl-3-(3-dimethylaminopropyl)-carbodiimide hydrochloride
FT-IR	Fourier transform Infrared spectroscopy
IgG	Human Immunoglobulin G
LbL	Layer-by-layer
LRSPR	Long range surface plasmon resonance
MPS	3-Mercapto-1-propanesulfonic acid sodium salt
NHS	N-Hydroxysuccinimide
PAA	Polyacrylic acid
PAH	Poly(allylamine hydrochloride)
PBS	Phosphate buffered saline
PDADMAC	Poly(diallydimethylammonium chloride)
PSP	Plasmon surface polarions
PSS	Poly(styrene sulfonate)
QCM	Quartz crystal microbalance
SEM	Scanning electron microscope
SPR	Surface plasmon resonance

LIST OF ABBREVIATIONS and SYMBOLS (CONTINUED)

TE	Transverse electric
TM	Transverse magnetic
WCSPR	Waveguide-coupled surface plasmon resonance
θ	Angle
ω	Surface plasmon frequency
d	Thickness
k	Wave vector
◦C	Degree of Celsius
ε	Dielectric constant

CHAPTER 1

Introduction

In recent years, the applications of the sensors have attracted attention in various fields including in electrical appliances and automobiles. The primary role of these sensors intended to measure the physical quantities such as heat, light, pressure, etc. It is called a physical sensor, on the other hand, is referred to a chemical sensor which is a sensor for measuring the chemical. In this work, we reported the fabrication of the layer-by-layer (LbL) water-stable electrospun polyacrylic acid (PAA) fibers based long range-surface plasmon resonance (LR-SPR) immunosensor for detection of human immunoglobulin G (IgG). The water-stable electrospun PAA fibers were fabricated by adding β-cyclodextrin as crosslinker in an aqueous PAA solution followed by heat treatment. A mixture of PAA and β-cyclodextrin was electrospun onto a gold-cytop coated high refractive index glass substrate (so called LR-SPR sensor chip) which then used for enhancing the signal of the sensor in LR-SPR immunosensor. The electrospun PAA fibers can enhance the signal of LR-SPR based immunosensor and bind with human IgG within the penetration depth of surface plasmon field around 1 μm. Moreover, the electrospun PAA fibers with high surface area on the sensor chip showed the advantage for increasing the surface area of the substrate hence increasing the number of sensing site (active carboxylic groups). Furthermore, for increasing sensing sites and also water-stability of the electrospun PAA fibers, multilayers of negative charge PAA and positive charge poly(diallyldimethylammonium chloride)

(PDADMAC) films were fabricated on the fibers by LbL deposition technique. The LR-SPR spectroscopy was employed to monitor the kinetic of the deposited PAA fibers and the stability of electrospun PAA fibers in PBS solution comparing with the conventional SPR spectroscopy. The water-stable electrospun PAA fibers with multilayers PAA/PDADMAC based LR-SPR immunosensor was finally constructed using monoclonal anti-human immunoglobulin G (IgG) as model antibody which can be used for probing the binding of human IgG with various concentrations.

1.1 Biosensor [1−13]

A biosensor is a device that makes of a biological detection system. Recently, biosensors are developed to convert the biological data to electrical signal. Biosensing is the process of using biosensors to gather information about living systems. According to IUPAC definition [1], "A biosensor is a self-contained intergrated device which is capable of providing specific quantitative or semi-quantitative analytical information using a biological recognition element (biochemical receptor or enzyme, antibody, or DNA) which is in direct spatial contact with a transducer element. A biosensor should be clearly distinguished from a bioanalytical system, which requires additional processing steps, such as reagent addition. Furthermore, a biosensor should be distinguished from a bioprobe which is either disposable after one measurement, i.e. single use, or unable to continuously monitor the analyte concentration"

In 1962, Clark and Lyons [2] described the first biosensor which glucose oxidase (GOD) was immobilized on an amperometric oxygen electrode surface semipermeable

dialysis membrane in order to quantify glucose concentration in a sample directly.

As shown in Figure 1.1, a biosensor consists of 2 main elements: (1) a bioreceptor, which is an immobilized sensitive biological element such as enzyme, DNA, antibody, recognizes the target analyte (enzyme substrate, complementary DNA, antigen) and (2) a transducer, for converting the biochemical signal to electrical signal. Moreover, types of biosensor are classified by (1) type of transducer (electrochemical, optical, piezoelectric and thermal), (2) type of bioreceptors (antibody, enzymes, nucleic acids), and (3) type of physical and chemical interaction. Some of the most commonly used are described in details below.

1.1.1 Conductometric biosensors [3–5]

Conductometric biosensors measure the changes in the conductance between a pair of metal electrodes as a consequence of the biological component. The measurement of conductance can be fast and sensitive. Such biosensors are suitable for miniaturization since the reference electrode is not required in the system. However, the selectivity of conductometric biosensors is relatively poor.

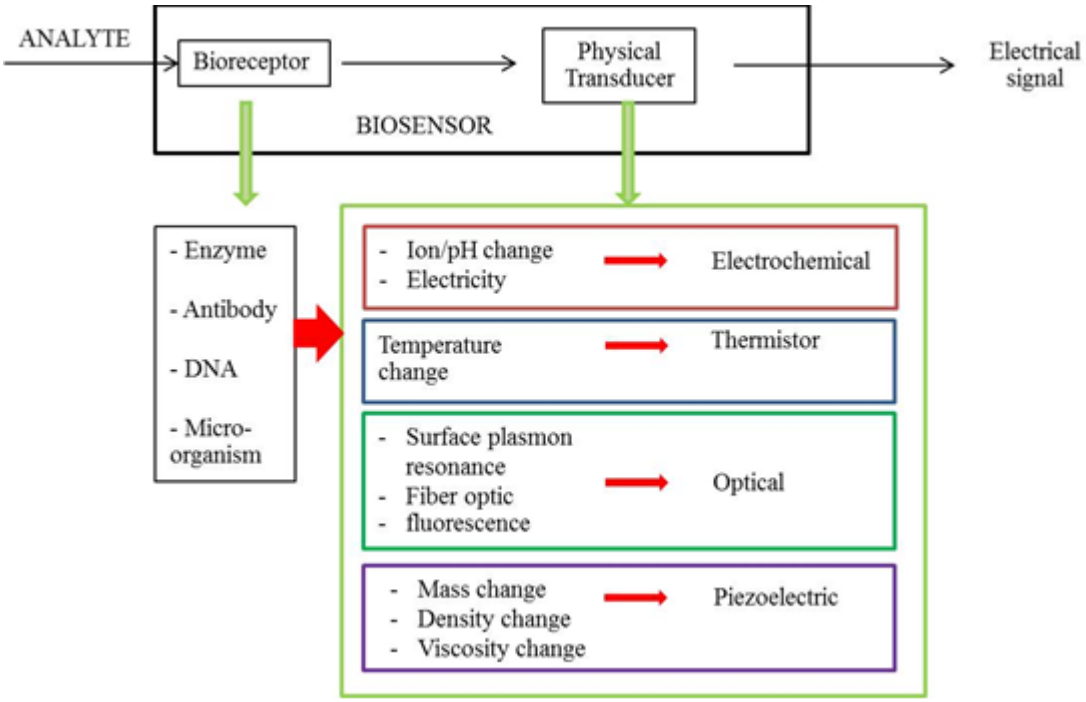

Figure 1.1 The diagram of biosensor [3].

1.1.2 Potentiometric biosensors [6–7]

Potentiometric biosensors consist of measurement of potentials at the working electrode with respect to the reference electrode. The function under equilibrium conditions and the accumulation of charge, at zero current, created by selective binding can be measured at the electrode surface. For example, ion selective electrode (ISE) can detect ions such as Na+, K+, Ca+, H+ of NH4+ in complex biological matices by sensing the changes in electrode potential when the ions bind to an appropriate ion exchange membrane. The sensitivity and selectivity of potentiometric biosensor are outstanding due to the species-selective working electrode used in the system. However, a stable and accurate reference electrode is required.

1.1.3 Amperometric Biosensors [8–9]

Amperometric biosensors measure the changes in the current on the working electrode due to direct oxidation of the products of a biochemical reaction. Amperometric techniques are linearly dependent of analyte concentration and give a normal dynamic range and a response to errors in the measurement of current. An amperometric biosensor was constructed by immobilization of hemoglobin onto a carboxylated MWNTs/copper nanoparticle/polyaniline composite deposited onto pencil graphite electrode which exhibited remarkably enhanced sensitivity and selectivity for acrylamide [8]. Cholesterol was immobilized on 2-(4-fluorophenyl)-4,7-di(thiophene-2-yl)-1H-benzo[d]imidazole deposited on a graphite electrode. The amperometric response was finally measured [9].

1.1.4 Piezoelectric Biosensor [10–11]

Piezoelectric measurements use the appearance of an electrical polarization, or a variation in an existing polarization, in certain anisotropic dielectric materials, for example, quartz. This polarization appears when a force is applied in the appropriate direction. The piezoelectric effect is reversible because the material can deform of vibrate when an electric field is applied in the appropriate direction. Piezoelectric devices are used at their resonance frequencies for the determination of small variations in mass. These variations may result from biological reactions that involve association or coupling, for example, enzyme-inhibitor associations or antigen-antibody coupling.

1.1.5 Optical Biosensor [12–13]

Optical biosensors that exploit light absorption, fluorescence, luminescence, reflectance, Raman scattering and refractive index are powerful alternatives to conventional analytical techniques as shown in Figure 1.2. These biosensors provide rapid, highly sensitive, real-time, and high-frequency monitoring without any time-consuming sample concentration and/or prior sample pre-treatment steps. The optical biosensors have great potential applications in the areas of environmental monitoring, food safety, drug development, biomedical research, and diagnosis. Surface plasmon resonance based biosensor, one type of optical biosensors, was studied in the next chapter.

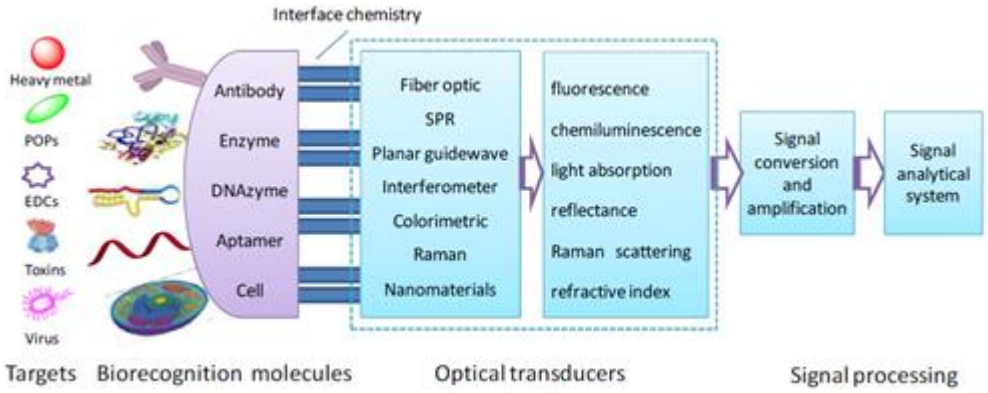

Figure 1.2 Schematic of an optical biosensor [13].

1.2 Electrospinning [14–35]

Electrospinning is a technique which employed for preparation of fibers with diameter in the range from micrometers down to nanometers scale depending on the polymer and processing conditions [14]. The electrospun nanofibrous films are formed

with high surface-to-mass ratio and small pore sizes. While this technique is quite complicated and having low productivity, the electrospun nanofibrous films exhibit much more interesting properties especially in the nanocomposite film viewpoint. In other words, electrospinning is a process that creates nanofibers through an electrically charged jet of polymer solution or polymer melt. The electrospinning process consists of a pipette to hold the polymer solution, 2 electrodes, and a high voltage supply as shown in Figure 1.3. The polymer drop from the tip of the pipet was drawn into fiber due to the high voltage. The jet was electrically charged and the charge caused the fibers to ben in such a way that every time the polymer fiber loop, its diameter was reduced. The fiber was collected on the ground electrode surface.

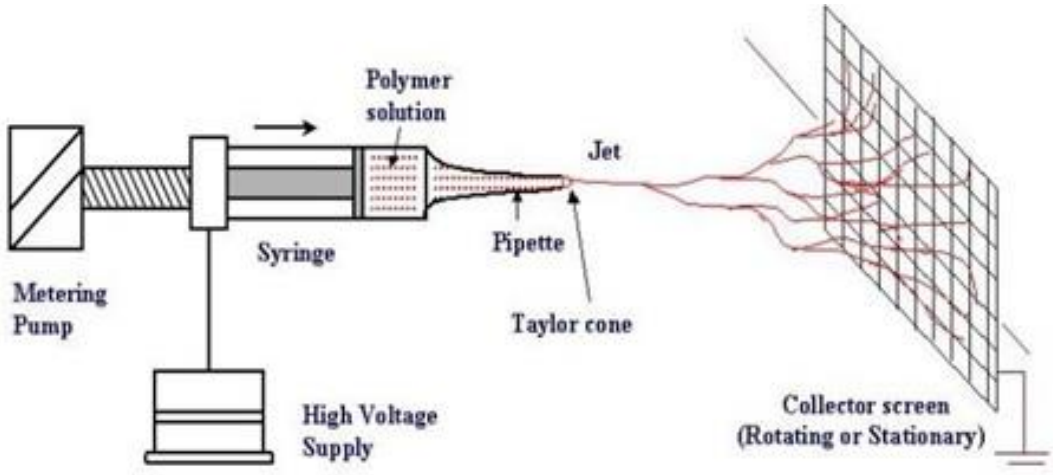

Figure 1.3 The electrospinning setup [20].

There are many parameters affecting the fibers morphologies during the electrospinning process. The parameters influenced the electrospinning process can be divided into 3 parts as shown in Table 1.1. The details are also described below.

Table 1.1 The parameters affected the electrospinning process [21].

Main parameter	Description
Solution properties	- Viscosity - Surface tension - Electrical conductivity - Polymer concentration - Molecular weight of polymer
Processing conditions	- Applied voltage - Distance between needle and collector - Feed rate - Needle diameter
Ambient conditions	- Temperature - Humidity

1.2.1 Solution parameters

Solution parameter is a main factor which affects the electrospinning process and morphology of the fibers. The concentration of the polymer solution is the one of important factor. At the very low concentration, the polymer solution with low viscosity

and high surface tension is exhibited the droplet instead of the fiber. When the concentration is higher, there are beads on the obtained fibers but in case of suitable concentration, the smooth nanofibers can be obtained. The very high concentration of the polymer solution causes the larger size of electrospun fibler, not in nanoscale. Moreover, the lower molecular weight of the polymer made the fiber with beads whereas smooth fiber can be obtained with increasing the molecular weight of polymer. Therefore, molecular weight of the polymer affects the length of polymer chain.

The other solution property which shows the important role for fiber morphology is solution viscosity. The very low viscosity solution, the droplet could be obtained due to lack of sufficient chain overlapping with the polymer solution, whereas the very high viscosity solution results in the hard ejection of jets from solution. For the suitable solution viscosity, the long chain, continuous and smooth electrospun fibers without any beads can be obtained.

In the initial of the electrospinning process, the polymer solution is come out from the tip of the tube to the ground collector by applying the high voltage. The electrostatic forces on the polymer chain in the solution must be strong enough to force the surface tension of the solution because the surface tension of the solution may cause the bead formation. The surface tension decreased the surface area per unit mass of the solution. The lower viscosity or higher amount of solvent molecule leads to spherical shape for minimizing the surface energy.

Another important parameter is conductivity of the polymer solution which is mainly determined by the polymer type, solvent, and ionization of salt. Electrospinning involves stretching of the solutions caused by repulsion of the charges at the surface.

Thus, if the conductivity of the solution is increased, more charges can be carried the polymer jet. The higher conductive polymer solution contains high electric charges during the electrospinning process which generates a stronger repulsive force that easier to form the bead-free and uniform electrospun fibers. The conductivity of solvents can be increased by addition of salts or non-chemical reaction compounds. When the conductivity of the solution is increasing, the thinner fibers can be obtained.

1.2.2 Processing parameters

The processing parameters including an applied voltage, a distance between needle and collector, feed rate, and a needle diameter are also important for electrospinning process. The high voltage will induce the charges on the solution and together with external electrical field to initiate the electrospinning process. At the applied voltage higher than the threshold voltage, the electrostaitc repulsive force will increase and the greater amount of charges will cause faster jet, less stable Taylor cone and smaller fiber diameter. However, the applied high voltage must correspond to feed rate to maintain the stable Taylor cone. The increasing feed rate in suitable feed rate can promote the greater of fiber diameter or bead size due to greater volume of solution drawn from the needle tip.

Moreover, during the electrospinning process, the one of the most important parameter is the collectors which usually act as the conductive as the conductive substrate to collect the charged fibers. An aluminum foil is employed as a collector but it is difficult to transfer the collected nanofibers to other substrates. In addition, the distance between tip and collector relates to the electric field strength. At the shorten

distance, the electric field strength will increase at the same time as the acceleration of jet is increased. Therefore, there is not enough time for solvent to evaporate before reaching the collector, then fibers fuse together to form web. If the distance is too short, the fiber will not have enough time to solidity before reaching the collector, whereas if the distance is too long, the bead fiber can be obtained.

The advantages of electrospinning are simple, convenient and reproducible method, cost effective, and long continuous nanofibers can be produced, however, jet is not stable [22–26]. The nanofiber formation depends on the properties of polymer solutions and the electrospinning factors such as applied voltage, the concentration of polymer solutions, collection distance, and flow rate of the solution. Li et al. [23] reported that the aqueous poly(acrylic acid) (PAA) with lower concentration as well as lower voltage could support continuous fiber formation, thinner fibers, and the obtained averaged size about 80 to 500 nm. The PAA fibers could be insoluble in water by adding β-cyclodextrin in the aqueous PAA solution followed by thermal treatment at 140 °C for 20 min. The obtained nanofibers showed very small diameter, large surface area per unit mass and small pore size. Due to these properties, the polymer nanofibers have been widely used in drug delivery systems, tissue engineering, sensor, catalytic films [27–30]. The electrospun nanofibers have been interested for sensor applications because their large surface area can enhance reactivity and sensitivity of the sensors. In addition, the large surface area will adsorb more amount of an analyte comparing with the film-type sensors [31–34]. In biomedical application, the surfaces of electrospun

fibers have been chemically and physically modified with bioactive molecules and cell recognizable ligands after the electrospinning process [35].

1.3 Long range-surface plasmon resonance (LR-SPR) spectroscopy [36–69]

Surface plasmon resonance (SPR) spectroscopy has been widely used in the last 10 years for biosensors or biomedical applications due to real time measurement, rapid monitoring binding and process without label or label-free of biomolecules. It has been applied to characterize biomolecular interactions, monitor the assembly process of molecules, study the conformational change of protein molecules and chemical transformations on the surfaces [36–41]. In sensor application, the principle of the SPR is based on a monitoring on the optical thickness change in refractive index and/or change in the thickness at the area close to the sensor surface. The plasma of free electrons will oscillate at an interface of metal after an angle of incident light larger than the critical angle so that it undergoes total internal reflection. The oscillations are affected by the refractive index of the metal thin film and media interface. The evanescent electromagnetic wave is generated in a region of non-conducting material and determines the limitation for detecting the mass change. Resonance occurs when the momentum and energy of the evanescent electromagnetic wave match with the momentum and energy of the surface plasmon. These can be characterized by a sharp decrease in intensity of the reflected beam as its energy is transferred to the surface plasmon. The application of SPR is to use for detecting the refractive index change on the metal surface owing to the change of mass on surface. These optical responses can be applied to measure the progress of the chemical interaction through the monitoring

of the changes in the effective refractive index or the mass coverage on the sensor surface. The sensitivity of the SPR immunosensor for detection of antigen-antibody interaction with very low analyte concentration can be increased by controlling the orientation of the antibodies on sensor surface and preservation of its structure in the active form [42−44].

SPR is a term to explain the phenomenon about narrow dark bands in the diffracted spectrum of metallic gratings illuminated with polychromatic light which Wood reported in early 1902 [45–46]. In 1968, Otto introduced the optical excitation of surface plasmons by attenuated total reflection [47]. SPR is a technique which associated with the total internal reflection of light (evanescent wave) at the boundary between two media of different optical properties described by their different dielectric function, ε_i [48]. The example of this observation is the boundary between a glass prism and water. A plane wave from a laser light source (wavelength, λ) or incoming light impinging upon the interface from glass side, i.e. from material with higher refractive index, will be totally (internally) reflected if the angle of incidence exceeds a critical value. This can be observed by recording the reflectivity (R, the ratio between reflected and incoming intensity) with a diode detector as a function of the angle of incidence, θ. In typical experiment, at angles of incidence smaller than critical angle, most of incoming light is transmitted and therefore the reflectivity is low. When the angle of incidence approaches critical angle, the reflectivity reaches unity. The evanescent wave is an electromagnetic field which the electric field perpendicular to the interface does not fall to zero abruptly but decays exponentially with a decay length. This decay length is a function of the angle of incidence. On the other hand, the component along the

propagation direction had the usual oscillatory character of an electromagnetic mode. The evanescent wave is formed at the angle greater than critical angle. When the interface between a metal and a dielectric material is considered, the term “plasmon surface polaritons (PSP) or surface plasmons” for short was described. The coupling of the collective plasma oscillations (called “plasmon”) of the nearly free electron gas in a metal to an electromagnetic field has been shown to produce the surface plasmon. This surface plasmon propagates at the metal/dielectric material with the coupling angle which can be excited with photons when the energy and momentum matching conditions between photons and surface plasmons has reached [48–51].

There are 3 coupling configuration of SPR sensors: grating, prism and optical waveguide based SPR sensor. The prism coupler-based SPR sensor (also called attenuated total reflection-ATR method), developed by Kretschmann, is most widely used in SPR sensor application. When the incident light passed through the prism and reached the interface between the prism and medium, the total reflection will occur, if the incident angle is larger than the critical angle. The reflected light is detected by detectors. The incoming light is able to couple with the surface plasmon in the metal at the angle of the incidence and the surface plasmon is excited.

Grating coupler-based SPR sensor was first developed in 1983 by Lukosz [52]. The grating replaces the need for a glass prism in traditional SPR. The grating is covered with gold. The light source illuminates the surface of the chip and the reflected light is captured by a CCD camera. By varying the incidence angle and measuring the reflected light intensity, a binding curve is created. Lower production costs and more latitude in selection of construction materials favor the use of gratings, particularly when design

versatility and high production volumes are considered. While many grating shapes can produce SPR, the optimal surface geometry is a sinusoidal grating. The period (peak-to peak dimension) and the amplitude (peak-to-trough dimension) of the grating determine the wavelength of resonance.

Coupling optical waveguide has some attractive features such as low cost, small device size which provides a simple way for controlling the optical wave path, ruggedness and suppression of the effect of stray light. The process of exciting a surface plasma wave in an optical waveguide-based SPR sensor is similar to that in the prism coupler-based SPR. A light wave is guided by the waveguide and, entering the region with a thin metal overlayer, it evanescently penetrates through the metal layer. If the SPW and the guided mode are phase-matched, the light wave excites an SPW at the outer interface of the metal. Theoretically, the sensitivity of waveguide-based SPR devices is approximately the same as that of the corresponding ATR configurations.

The different configurations by using prism have been widely used for many applications. In principle, there are two concepts for this experimental setup: Otto-configuration and Kretschmann configuration as shown in Figure 1.4. The Kretschmann is the most widely used and convenient configuration because the resulting plasmon can be observed directly through the metal. In the Otto-configuration, the order of layers is glass substrate, air gap, metal layer, glass substrate, and liquid. The photons are not couple directly to the metal/dielectric interface, but via the evanescent tail of light totally internally reflected at the base of a high-index prism ($\varepsilon_p > \varepsilon_d$). By choosing the appropriate angle of incidence, resonant coupling between evanescent photons and surface plasmons can be obtained. This resonant coupling is

observed by monitoring the laser light, which is reflected by the base of prism, as a function of the incident angle. However, the metal surface should close enough to the prism base, typically ~ 200 nm. This means even a few dust particles can be the spacers preventing the efficient coupling. Due to this limitation, the Otto-configuration has not gained any practical importance despite its potential application for the optical analysis of polymer coated bulk metal samples. On the other hand, in Kretschmann configuration (Figure 1.4 (b)), the order of layers is a metal layer sandwiched between glass substrate and liquid. The photons in the prism coupled through a very thin metal layer (typically ~ 45–50 nm thick), which is deposited directly onto the base of the prism or onto a glass slide, to surface plasmons at the other side in contact with the dielectric medium. In qualitative, the same consideration for energy and momentum matching are applied as discussed in Otto configuration. Quantitatively, however, the finite thickness of the metal layer causes some modification of the dispersion behavior at surface plasmons. By solving Maxwell's and/or Fresnel's equations for the layer architecture of glass/Ag-layer/ dielectric, the angular dependence of the reflectivity can be described.

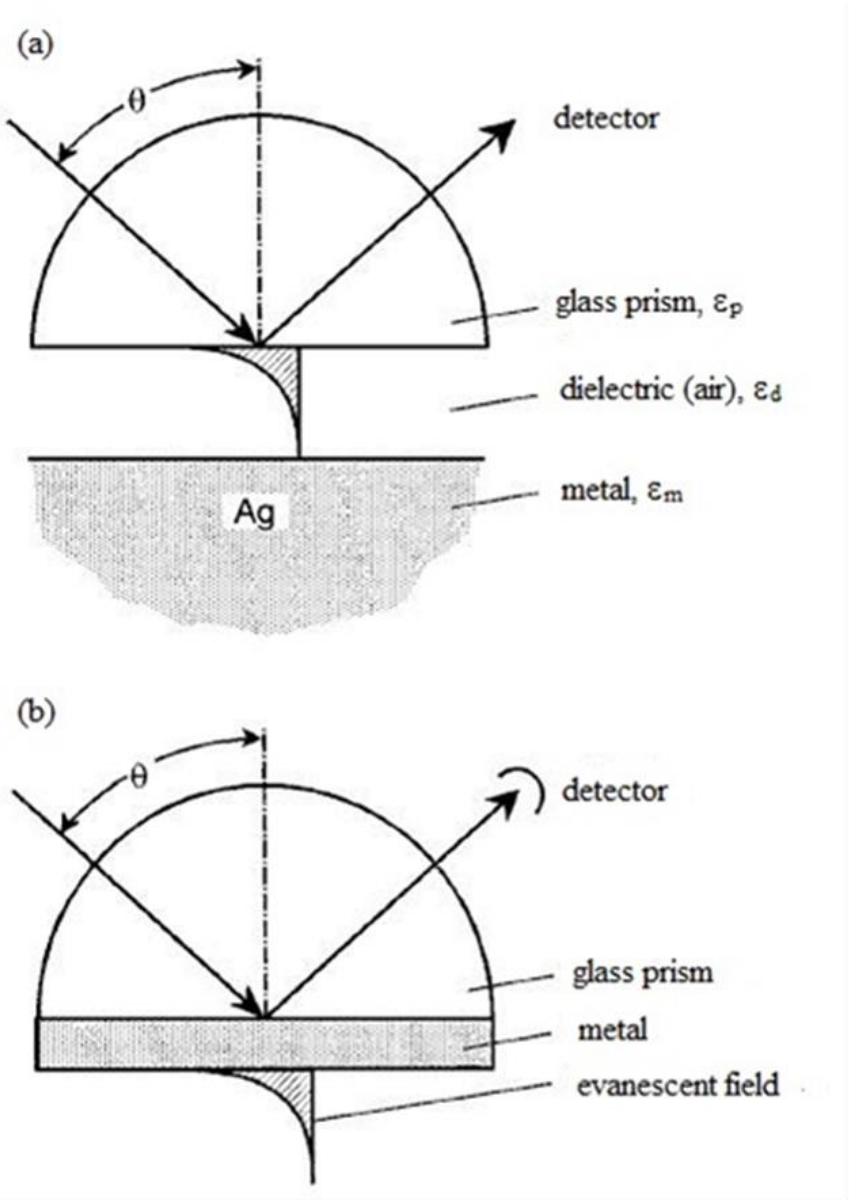

Figure 1.4 Two concepts for experimental setup of surface plasmon resonance spectroscopy (a) The Otto-configuration (b) Kretschman configuration with attenuated total internal reflection (ATR) construction [48].

In classifying biosensors which utilize the electro-magnetic field enhancement of SPR excitation near the surface of a metal thin film, four basic types can be identified, namely the conventional SPR, the long range-SPR (LR-SPR), the coupled plasmon-waveguide resonance (CPWR), and the waveguide-coupled SPR (WCSPR), as shown in Figure 1.5. The LR-SPR biosensor introduces a dielectric buffer layer between the prism and the metal layer of the conventional SPR biosensor. A symmetric environment is achieved when the refractive indexes of the dielectric buffer layer and the buffer are equal, with the result that the propagation length of the SPs increases beyond that of the conventional one and the energy of the incident beam is retained. The LR-SPR device exhibits a very sharp (i.e. large depth-to-width ratio) reflectivity dip, which increases the signal-to-noise ratio and enhances its resolution by approximately seven times compared to the conventional SPR under wavelength interrogation. However, since the performance of the LR-SPR relies upon the existence of a symmetric environment, the device is not readily applied to the different detective environments associated with variant biomolecules or buffer solution. CPWR biosensors incorporate a waveguide layer beneath the surface of the conventional SPR biosensor. Unlike the conventional SPR biosensors, whose reflectivity spectra demonstrate a dip only in the transverse magnetic (TM) mode, the interference of the waveguide layer in the CPWR device causes sharp dips in both the TM and transverse electric (TE) modes. These dips reduce the noise and greatly increase the SNR. The TM and TE reflectivity spectra of the CPWR device can provide the information required to determine the dielectric constant and thickness of the biomolecular layer. Although CPWR biosensors possess significant advantages in the study of anisotropic membrane

systems, their sensitivity is still some 10 times less than that of conventional SPR devices since the biosensing surface is located at a considerable distance from the SPs which exists at the interface between the metal film and the waveguide layer. Therefore, it is difficult to determine variations in the dielectric constant and thickness from the dips of the CPWR TE and TM reflectivity spectra if the biomolecular layer is slightly variable. Unlike the LR-SPR with its coating of a special dielectric buffer layer, a WCSPR consists of two metal layers and a waveguide layer. Combining the SPR and waveguide modes in the WCSPR device not only retains the sensitivity of the biosensor, but also yields sharper reflectivity spectra dips which enhance the measurement precision. The WCSPR biosensor provides increasing intensity measurement sensitivity, and measurement of the two WCSPR dips provides sufficient information to precisely determine the dielectric constant and thickness of the biomolecular layer.

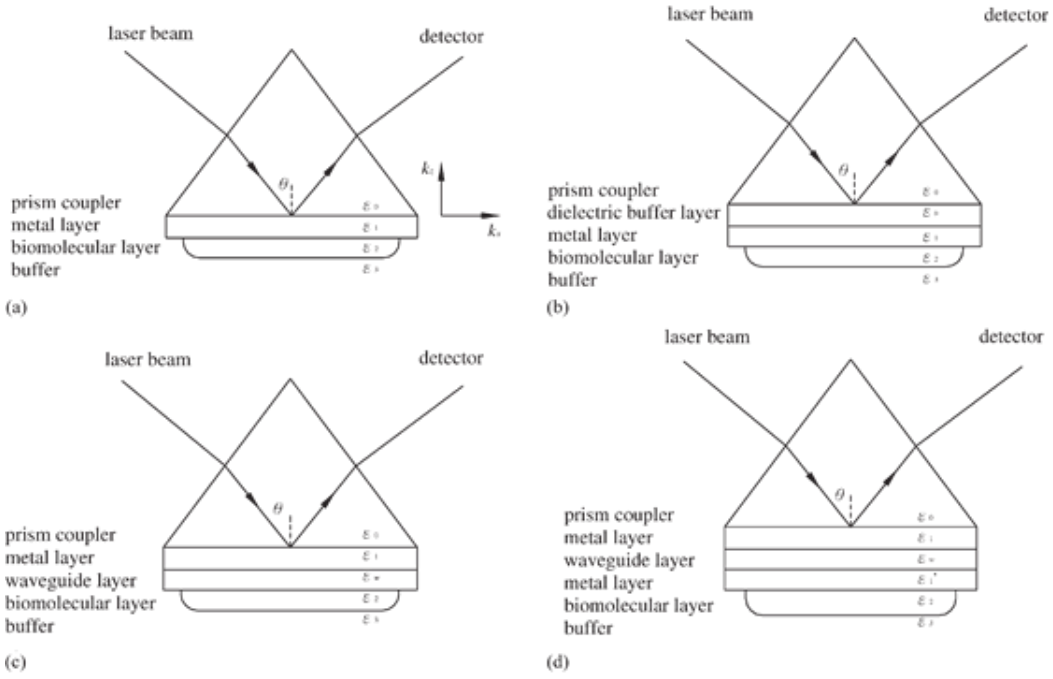

Figure 1.5 Configurations of four different SPR biosensors: (a) conventional SPR (b) LR-SPR biosensor (c) CPWR (d) WCSPR [53].

SPR has been shown to be a technique which has high sensitivity for characterization of ultrathin film, interfaces, and kinetic processes at the nanometer scale [48, 51, 54]. Hence, if the condition of light excitation is fixed, the SPR technique not only permits the precise measurement of changes in the refractive index or thickness of the medium adjacent to the metal film, but also enables changes in the adsorption layer on the metal surface to be detected. The experimental SPR system for characterization of ultrathin films which relatively simple was shown in Figure 1.6(a), a laser beam of wavelength λ incidents at angle θ on the noble metal coated base of the prism, which is covered with the thin film of interest material, is reflected. The intensity

of the reflected light is then monitored with a detector as function of θ. Figure 1.6(b) showed the reflectivity curves, first is the curve label taken in air on a bare Au-film evaporated-deposited onto the prism base and second is the curve of an ultrathin organic layer of interest molecules on Au surface which can be prepared by spontaneous self-assembly process such as Langmuir-Blodgett (LB) technique, layer by layer (LbL) deposition method or simple technique such as spin-coating, results in a shift of the curve for PSP running along this modified interface and hence in a shift of the resonance angle (from θ to θ_1). The example for using of SPR to in situ investigation of the self-assembly polymer solution adsorption process was studied by Knoll group [51].

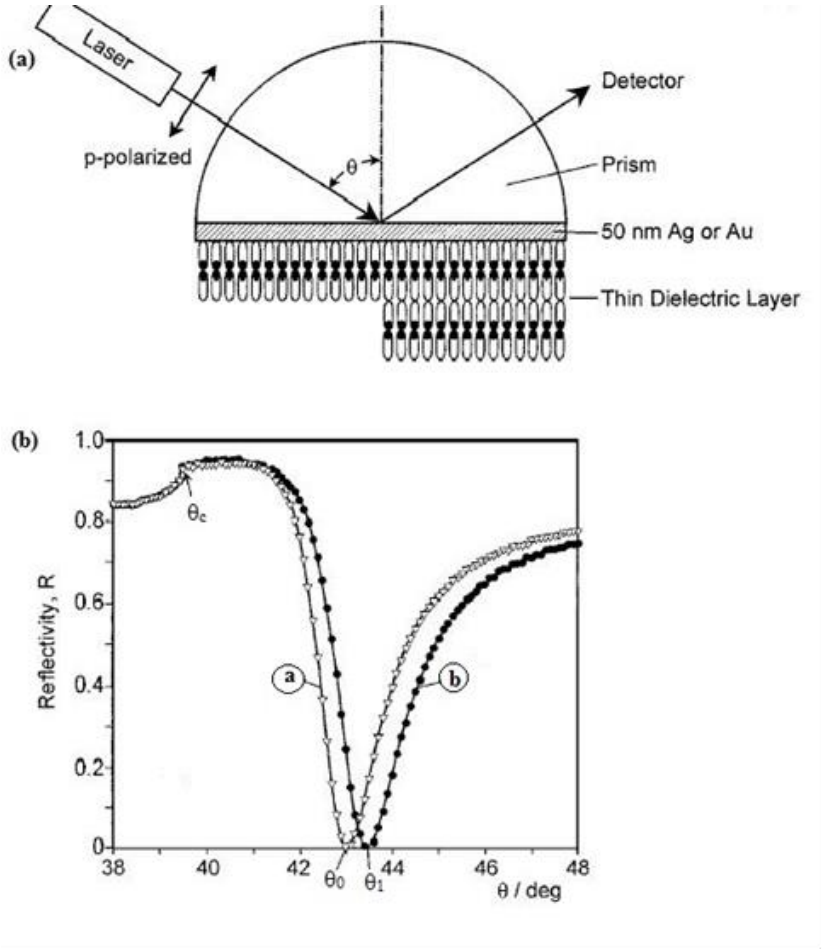

Figure 1.6 Schematic of (a) the experimental SPR system for characterization of ultrathin film for (b) SPR reflectivity curve obtained from a bare Au-film and self-assembled monolayer [48].

The experimental setup in this study is Kretchmann configuration with ATR condition. The monolayers of each interest materials were stepwisely deposited by LB process onto the high refractive index glass/Au/octadecyl-thiol layer. A sequence of reflectivity data taken after consecutive depositions showed the linear increases of the

multilayer thickness after analysis with Fresnel equation [51]. In addition, the other data, which can be obtained by using SPR, is the kinetic data on the interfacial of the multilayer. The kinetic information on any changes of the interfacial architecture is the time-dependent process which can be obtained by monitoring the reflectivity at a fixed angle of observation, as shown in Figure 1.7. At t = 0, no change occurs at the sensor in the buffer solution. After the solution is injected, the biomolecules will adsorb on the surface and resulting in a change in reflectivity. The adsorption-desorption of the biomolecule can be followed in real time.

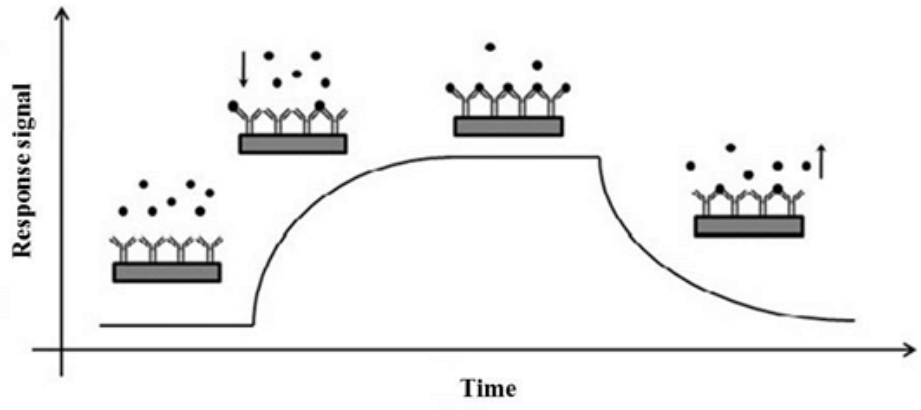

Figure 1.7 The SPR kinetic at the fixed angle [55].

Conventional SPR spectroscopy is the one famous technique for use in sensor application due to its direct, label-free observation of biomolecular interaction. The high resolution of the sensor can be detected the low concentration of the biological agents. The resolution of the SPR sensor can be improved by decreasing the width of

the resonance feature, reducing the uncertainty of the position of the resonance and increasing the sensitivity of the sensor. The one method for increasing the resolution is using silver or gold as metal layer but silver is poor for the long-term stability in environments. Another method is using long-range surface plasmon resonance (LR-SPR) spectroscopy which decreasing the resonance width and increasing the sensitivity of the sensor.

LR-SPR is one mode of surface plasmons (SPs) that propagating along a thin metallic film embedded between 2 dielectrics with similar refractive indices, where the evanescent field intensity and the penetration depth are larger as compared to the well-known short range (SR)-SPs evanescent field [56 - 61]. The longer propagation length of LR-SP reduces the width of the resonance feature. Moreover, the LR-SPR sensor may provide higher sensitivity than the conventional SPR sensor at the same wavelength.

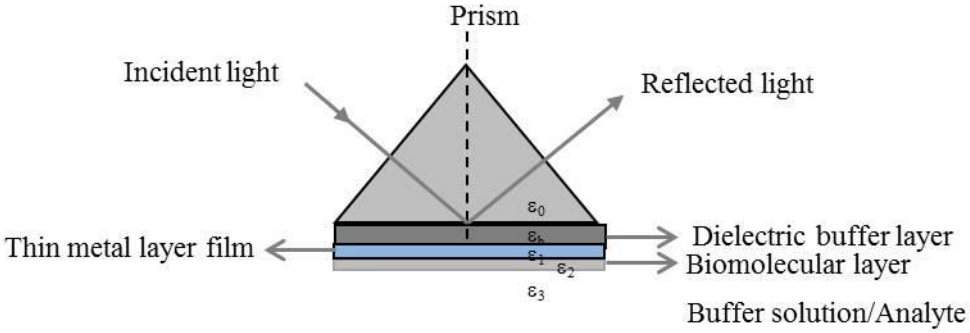

Figure 1.8 Schematic diagram of LR-SPR biosensor [54]ทำให้เป็นรูป ไม่ใช่กล่องข้อความ มันเลื่อน

Chien *et al.* [54] and Nenninger *et al.* [62] reviewed the LR-SPR biosensor as following in Figure 1.8. LR-SPR biosensor based on the Kretschmann configuration consists of 5 typical layers which are prism (ε_0), dielectric buffer layer (ε_b, d_b), thin metal layer (ε_1, d_1), biomolecular layer (ε_2, d_2), and buffer/analyte layer (ε_3). In the devices, the thin metal layer is separated from the ATR prism by an additional dielectric buffer layer with a lower refractive index than the prism and similar dielectric constant to the intended buffer. A symmetric environment is achieved on either side of the thin metal layer. Ideally, the dielectric constants of the dielectric buffer layer and the analyte solution will be the same value ($\varepsilon_b = \varepsilon_3$). For biosensors, the analyte solution is generally aqueous, with a thin layer of protein on the surface of the sensor, therefore, a buffer layer with a refractive index near water is required. The refractive index of the buffer layer material is important parameter for LR-SPR sensor construction. The examples of buffer layer are Teflon AF-1600 and magnesium fluoride (MgF_2). The Teflon AF-1600 has a refractive index ($n_d = 1.31$) which is less than water ($n_d = 1.33$), while MgF_2 has a refractive index ($n_d = 1.38$) which is higher than water. The Teflon-buffer LR-SPR sensor would be preferable for low molecular weight functionalization layers, while the MgF_2-buffer LR-SPR sensor is more appropriate for higher refractive index, multiple-layer or polymer functionalization methods. The perturbing effect of the prism becomes more pronounced as the buffer layer becomes thinner, and may cause the resonant wavelength to shift or may prevent the LR-SP waveguide from being supported in certain wavelength ranges. Therefore, the first parameter for selection of the buffer is the thickness of the metal layer (typically gold) and the thickness of the

buffer layer. The operating angle of the instrument may be varied in order to produce the best coupling between the light and the LR-SPR, as indicated by a seep resonance with low TM reflectivity at the minimum of the resonance. Choosing a designed analyte provides an operating point for the sensor. Given these parameters, a designed curve may be produced displaying the best resonance depth, the wavelength at which this resonance occurs, the width of the resonance, and the sensitivity of the sensor. The construction of sensors with a thick Au layer and a thin buffer layer shows the resonant wavelength shifts to longer wavelengths as the refractive index of the analyte increases. In the case of sensors with a thin Au layer and a thick buffer layer, the sensitivity is negative, so the resonant wavelength shifts to shorter wavelengths with an increase in the refractive index of the analyte.

If the thickness of the thin metal layer is such that $k_{z1}d_1 << 1$ (k refer to wave vector and d refer to the thickness), the resulting symmetric configuration causes the same surface plasmon frequency (ω) to exist on both sides of the thin metal layer, and interaction then takes place between the electromagnetic fields of both surfaces. Under these conditions, the surface plasmon frequency divides into $\omega^{\pm}$. The electric field of the high-frequency ω^{+} mode is asymmetric to the center plane of the thin metal layer while the electric field of the low-frequency ω^{-} mode is symmetric to the same plane. The short-range dispersion relationship (L^{+}), and long-range dispersion relationship (L^{-}), for this symmetric configuration is given by Raeher in 1980 as shown below:

$$\omega^{+} : L^{+} = \varepsilon_1 k_{z3} + \varepsilon_3 k_{z1} \tanh\tfrac{1}{2}\mathrm{j}\, k_{z1} d_1 = 0$$

$$\omega^{-} : L^{-} = \varepsilon_1 k_{z3} + \varepsilon_3 k_{z1} \mathrm{ctgh}\tfrac{1}{2}\mathrm{j}\, k_{z1} d_1 = 0$$

These short-range and long-range surface plasmon modes are characterized by greater and lesser loss, respectively. Compared to the conventional SPR biosensor, the propagation length of the LR-SP is increased by a factor of approximately 10 times, the incident beam energy is more concentrated, and the depth-to-width ratio of the resonance dip is increased. The reflectivity minimum at a lower angle has a smaller half-width and hence indicates the long-range surface plasmon mode, while the dip at a higher angle is indicative of the short-range surface plasmon mode. Hence, it is expected to increase the sensitivity in the long distance from the metal surface. Berini [63] reported the difference between the refractive index of the surface plasmon mode and the dielectric decreases, causing the plasmon mode to be less confined in the metal layer, and extending the penetration depth of the evanescent field into the dielectric medium [64]. Therefore, LR-SPR compared with standard SPR shows a greater sensitivity to bulk refractive index variations in the dielectric medium [65]. The penetration depth of surface plasmon field for LR-SPR is around 1000 nm. Recently, Himola et al. [66] reported that penetration depth of the long range surface plasmon is 1400 nm in the device which can be detected for large size analytes such as bacteria, E.coli (with dimensions about 0.7- 1.0 μm) [67 - 68]. Moreover, LR-SPs enhancing the optical field wave at the metal/dielectric interface showed higher sensor sensitivity than conventional SPR and increased penetration depth reaching further into the analyte solution. This allows the use of thicker sensor coatings with significantly more binding analyte molecules on the surface [69].

In conclusion, LR-SPR shows the important advantages for optical biosensors application as shown below;

1) The long range mode of surface plasmon was excited at the lower angle than the conventional SPR which is very advantage for practical applications.
2) The LR-SPR optical field enhancement at the interface of the metal and dielectric buffer layer is more than an order of magnitude, which the sensor sensitivity can be enhanced.
3) The penetration depth of LR-SPR is higher than normal SPR mode which the thicker sensor coating can be used (thicker sensor led to more analyte molecules being coupled to the surface).

1.4 **Polyelectrolytes** [70–87]

Polyelectrolytes are polymers that contain electrolyte or ionizable groups which can be dissociated in aqueous solution as water and leaving charges on polymer chains and releasing counter ions in the solution. They are generally soluble in water. Polyelectrolytes are thus similar to both electrolytes (salts) and polymers (high molecular weight compounds) such as polystyrene sulfonate, polyacrylic and polymethacrylic acids and their salts, DNA, polyacids, and polybases. Electrostatic interactions between charges lead to the rich behavior of polyelectrolyte solutions different from uncharged polymers [70-72].

The polyelectrolytes are classified into various types. For example, based on their originals, polyelectrolytes were classified as natural, synthetic polyelectrolyte, and chemically modified biopolymer. Polyelectrolyte can be classified to polyacids/polyanions, polybases/polycations, and polyampholytes. Some important polyelectrolytes are shown in Table 1.2.

Table 1.2 Some of important polyelectrolytes [73]

Type	Name	Category
Natural polyelectrolyte	Nucleic acid	Polyanion
	Poly(L-lysine)	Polycation
	Poly(L-glutamic acid)	Polyanion
Chemically modified biopolymer	Pectin	Polyanion
	Chitosan	Polycation
	Cellulose-based	Polyanion or polycation
	Starch	Polyanion or polycation
	Dextrin	Polyanion or polycation
Synthetic polyelectrolyte	Poly(vinylsulfonic acid)	Polyanion
	Polyacrylic acid	Polyanion
	Poly(diallydimethyl ammonium)	Polycation
	Poly(styrene sulfonic acid)	Polyanion
	Maleic acid/diallyamine copolymer	Polyampholytic

Polyacrylic acid (PAA) was used as polyelectrolyte because of its wide range practical applications such as supplement to surfactants, used in the production of paper, inhibitor of fur formation, concentrators in cosmetics and components of drugs (artificial tears) [74]. A lower molecular weight PAA has been used as a dispersant whereas a higher molecular weight has been used as a thickener. The PAA with molecular weight of above 100,000 has been used as a flocculent. Moreover, PAA is an important weak anion polyelectrolyte which has been widely used in various

applications such as the metal ion complexing agents, a layer component for polyelectrolyte multilayer construction and sensors [75 - 78]. In sensing application, the carboxylic group of PAA was served as sensing probe to attach with analytes including gas sensors and biosensors [79 - 82]. Ding et al. [83] studied the nanofibrous membrane of PAA and water-stable PAA/polyvinyl alcohol (PVA) coated on quartz crystal microbalance (QCM) for use as a gas sensor. The PAA is acted as sensing materials for coating on QCM due to the interaction between ammonia gas molecules and carboxylic groups of PAA. The results indicated that the nanofibrous PAA coated on QCM showed higher sensitivity than the film coated on QCM in gas sensing. However, Lee *et al.* reported [84] that PAA layer in TiO_2/PAA ultrathin film which was LbL nanoassembled on QCM gas sensor for detection of amine odors can improve the intrinsic problems of QCM and binding of ammonia to their available carboxyl groups as the results of FT-IR measurements. The PAA and water-stable PAA showed the higher sensitivity in gas sensor which exhibited excellent performance to remove metal ion in an aqueous solution. However, in biosensing application, carboxylic groups of surface-tethered PAA brushes were immobilized to biotin which showed an enhanced signal for binding of streptavidin by using SPR spectroscopy. The PAA brushes showed very low non-specific interactions with other proteins [85, 86].

In addition to the bonds which hold monomers together in a polymer chain, many polymers form bonds between neighboring chains which called ‘crosslinking’. These bonds can be formed directly between the neighboring chains, or two chains may bond to a third common molecule. Though not as strong or rigid as the bonds within the chain, these crosslinks have an important effect on the polymer properties. Polymers with a

high enough degree of crosslinking show the ‘memory’ property. When the polymer is stretched, the crosslinks prevent the individual chains from sliding past each other. The chains may straighten out, but once the stress is removed they return to their original position and the object returns to its original shape.

The PAA crosslinked with β-cyclodextrin (CD) was synthesized by Kutyla [87, 88] for controlled delivery of drug releasing. The structure of crosslinked CD-PAA is shown in Figure 1.9. PAA can be crosslinked with CD via ester bonds formed between the sugar hydroxyl groups and the carboxylic acid groups of the polymers. The obtained crosslinked polymer is more stable than homopolymer PAA.

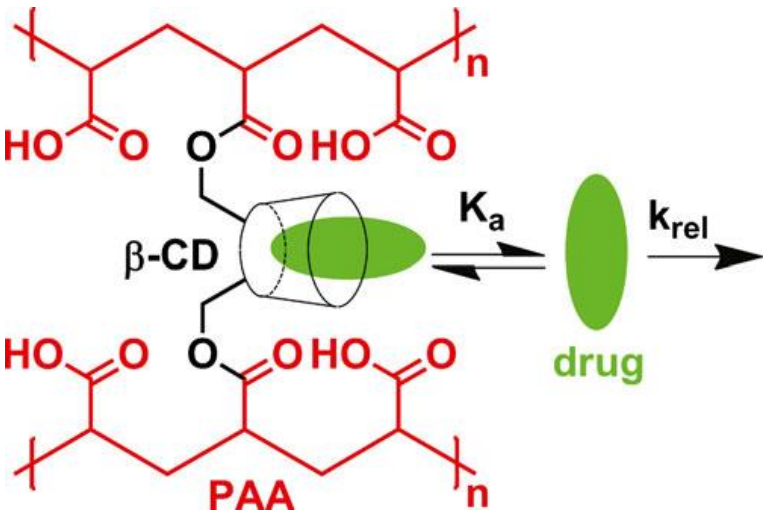

Figure 1.9 Structure of crosslinked CD-PAA polymer showing the kinetic of drug releasing [87].

Li *et al.* [23] reported the method to fabricate insoluble PAA. PAA fibers generally solubilize in water due to its polyelectrolyte property and carboxyl group on the backbone. However, crosslinked PAA is insolubilized in water by crosslinking with

β-CD followed by heat treatment. The results show the swelling property of the crosslinked polymer in aqueous solution.

1.5 Layer-by-Layer Deposition Technique [89–97]

Layer-by-layer (LbL) deposition technique is a thin film fabrication technique which the film is formed by deposition of the alternation layers of positively and negatively charged materials with washing during charge deposition. LbL deposition has interested in the preparation of well-ordered, ultrathin organic films for use as thin film coatings, electro-optic devices, and various display devices [89]. Decher *et al.* [90 - 92] developed this electrostatic LbL self-assembly technique in early 1990s for the construction of multicomposite films of rod-like molecules equipped with ionic groups at both ends, polyelectrolytes or other charged materials through the adsorption from aqueous solution. The LbL self-assembly technique has become a powerful method for fabrication of ultrathin films with uniform and controlled thickness. This method involves strong electrostatic attraction between a charged surface and the oppositely charged molecules (polycations and polyanions) which is the energetic driving force for multilayer formation [89, 92, 93]. The schematic diagram showing the fabrication of multilayers which compose of polyions or other charged molecules or colloidal objects (or both) is shown in Figure 1.10.

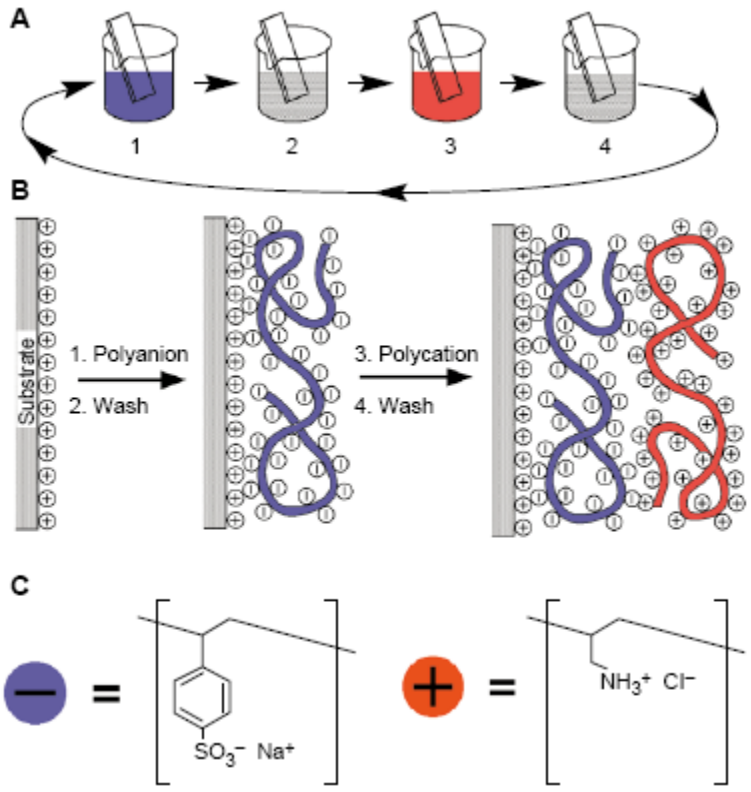

Figure 1.10 Schematic of the build-up of multilayers on a substrate by adsorption of typically polyanions and polycations. [92]

In principle, there is no restriction with respect to substrate size and topology due to the process involves only adsorption from solution. The ultrathin films are deposited on the substrate as shown in Figure 1.10(a). The glass slide substrate is immersed in the solution from ordinary beakers which can be performed either manually or by an automatic device. A well-cleaned substrate is first deposited with polyelectrolyte (positively charged in this example) prior to deposition of interested materials. This charged substrate is then sequentially immersed into the solution of polyanion and

polycation, respectively. A representation for the buildup of multilayer film at molecular level is shown in Figure 1.10(b). The counterions are omitted and the stoichiometry of charged groups between polyions and between the substrate and polyanion is arbitrary in this example. The two typical and commercial polyelectrolytes, sodium poly(styrene sulfonate) (PSS) and poly(allylamine hydrochloride) (PAH) are also shown in Figure 1.10(c). The concentration of the solution used in LbL method is in several milligrams per milliliter. These concentrations are much greater than that required for reaching the plateau of the adsorption isotherm to ensure that the solutions do not become depleted during the film fabrication which composes of several layers. In addition, one or more washing steps are performed after each layer adsorption to avoid contamination for the next adsorption solution by liquid adhering to the substrate from the previous adsorption step. The advantage of the washing step is to stabilize weakly adsorbed polymer layers. The appropriate adsorption times for each layer depend on the type of materials, molar masses, concentrations, and agitation of solutions which ranging from minutes in the case of polyelectrolytes to hours in the case of gold colloids.

The two major advantages of layer-by-layer adsorption from solution are as followed: (1) many different materials can be incorporated in individual multilayer films and (2) the film architectures are completely determined by the deposition sequence. Furthermore, no special film balance is required for this technique which indeed the technique has been referred to as a “molecular beaker epitaxy” [94]. Several applications of this technique have been reported due to its simplicity in processability, versatile and use of water-based solutions. Advincula group [89, 95, 96] reported the

preparation LBL ultrathin films of benzophenone-modified PAA (PAA-BP) and PAH (PAH-BP) for use as pH-responsive or pH-switchable membranes. The membranes can be produced by adjusting the pH of dipping solutions and stability maintained by crosslinking which showed high stability. Another work of Decher [92] showed the utility of LbL technique for fabrication of the multilayers of fullerenes such as C60 with polyamines. Baba *et al*. [97] fabricated single walled carbon nanotubes/organic semiconductor hybrid ultrathin multilayers by LbL self-assembly approach. Single walled carbon nanotubes was solubilized in cationic alcian blue pyridine variant and anionic copper phthalocynine-3,4′,4″, 4′ ″-tetrasulfonic acid tetrasodium salt. The results from *in situ* SPR spectroscopy indicating the successive formation of ultrathin films and single walled carbon nanotube can enhance the electroactivity of the hybrid film. Sriwichai *et al.* [98] also fabricated the ultrathin films of linear cationic sexithiophene (6TNL) and dendrimeric cationic sexithiophenes (6TND) with anionic polycarbazole precursor by LbL self-assembly deposition technique.

1.6 Instruments [99–101]

1.6.1 Surface plasmon resonance (SPR) spectroscopy

The typical prism coupling SPR based sensor is shown in Figure 1.11. Helium-Neon (He-Ne) laser beam of p-polarized light is focused on to the prism base using the lens and reflected light is measured using an ultrasensitive photodiode. The polarizer is set to polarize the incident beam as p-polarized in the direction parallel to the plane of incidence, in this case, in the horizontal plane. Surface plasmon is excited using Kretschmann configuration in which the metal film is in direct contact with the prism

base. Lock-in-amplifier and chopper are integrated with the proposed set-up to improve signal to noise ratio (SNR) of the measurement. A chopper is used to modulate the intensity of the incident light and the lock-in amplifier is employed to measure the data with reference to the chopping frequency. Gold film is used as the metal film, which is coated on the base facet of BK7 prism.

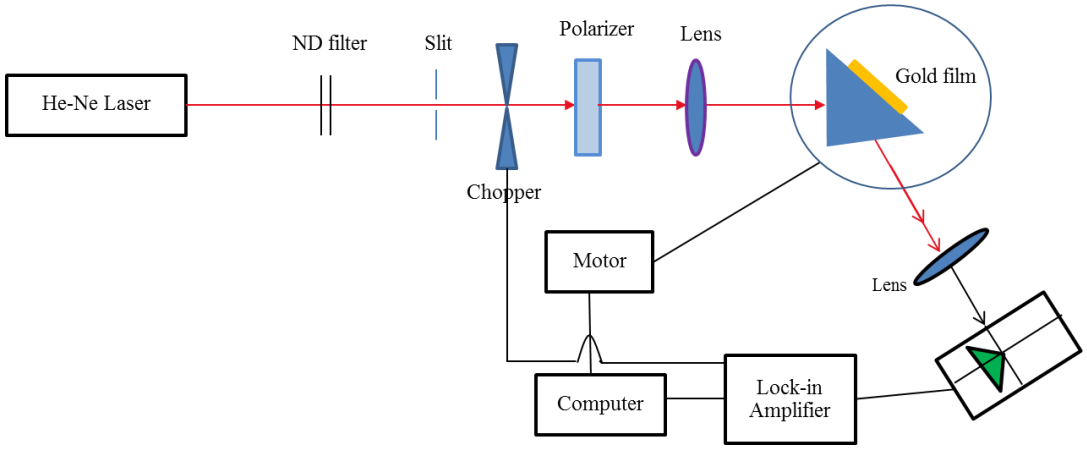

Figure 1.11 ATR set up. [99]

The prism is fixed on the rotation table and rotated in steps of 0.1° to change the momentum of incident light with respect to dielectric-metal interface. SP will be excited once the momentum between the incident light and surface plasmon is matched. Maximum energy transfer (K_{sp}) between photon to surface plasmon takes place at SPR angle and is very sensitive to dielectric property of the material adjacent to gold film which is given by

$$K_{sp} = \frac{\omega}{c}\sqrt{\frac{\varepsilon_m \varepsilon_d}{\varepsilon_m + \varepsilon_d}}$$

where ω is the frequency, c is the velocity of the light, and ε_1 and ε_b are dielectric constants of metal layer and dielectric buffer layer, respectively.

1.6.2 Scanning electron microscopy (SEM)

The first SEM was pioneered by Zworykin and co-workers in 1942 [100]. The instrument was further developed for the first commercial SEM by the Cambridge Scientific Instruments model Mark I, which was first commercially available in 1965. The SEM is one of the electron microscope instruments capable of producing high-resolution images of the sample surface and analysis of the microstructural characteristic of solid specimen. The basic components of the SEM are the lenses, electron gun, electron collector, visual and recording cathode ray tubes (CRTs) as well as the electronics with CRTs.

In the typical SEM as shown in Figure 1.12, the electron gun is the source for the electron beam used to probe the sample. Electrons emitted from a cathode which is a type of a tungsten or lanthanum hexaboride (LaB6), accelerated towards an anode. One or two condenser lenses for focusing the electron beam passes through pairs of scanning coils or pairs of deflector plates in the objective lenses. The electron beam is horizontally and vertically deflected by objective lenses. When the primary electron beam interacts with the sample, the electrons lose energy by repeated scattering and absorption within a teardrop-shape volume of the specimen. The signals of the greatest

interest are the secondary and backscattered electrons, due to these variations according to differences in surface topography as the electron beam sweeps across the specimen. The secondary electron emission is confined to a volume near the impact area of the beam, producing an image to be detected. A detector counts the secondary electrons and then amplifies them by photomultiplier tubes. The resolution of the SEM depends on the size of the electron spot, which in turn depends on the magnetic electron-optical system that used to produce the scanning beam. SEM requires sample to be conductive by coated with gold by a sputter coater.

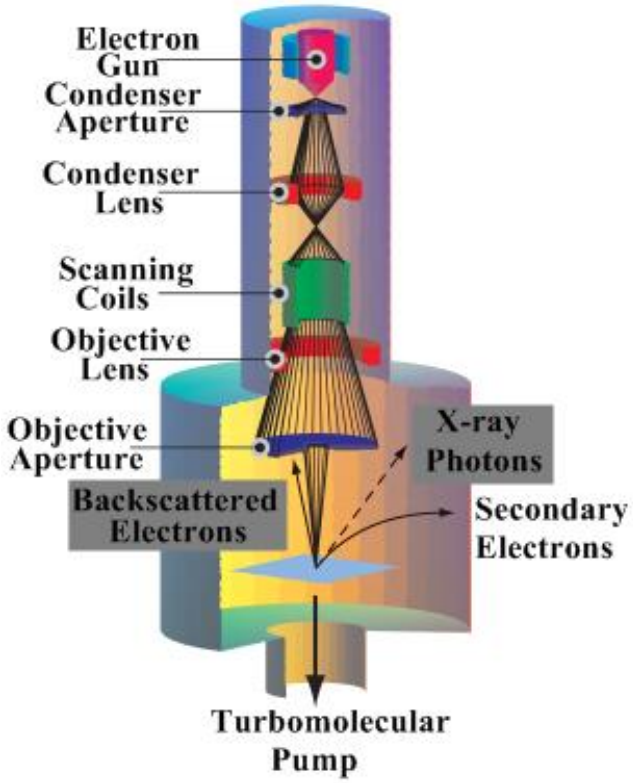

Figure 1.12 A schematic of Scanning Electron Microscope [101].

- At the top of the picture is an electron gun, producing a stream of monochoromatic electrons.
- The electron beam is condensed by the first condenser lens, which is used to form the beam. Together with the condenser aperture, it eliminates the high–angle electrons from the beam.
- The second condenser lens forms the electrons into a thin, tight, coherent beam and is usually controlled by the "fine probe current."
- A user–selectable objective aperture further eliminates high–angle electrons from the beam.
- A set of coils then "scans" or sweeps" the beam in a grid fashion like a television, dwelling on points for a period of time (usually in the microsecond range) determined by the scan speed.
- The final lens, the objective lens, focuses the scanning beam onto the desired part of the specimen.
- When the beam strikes the sample, interactions occur inside the sample and are detected by various instruments.
- Before the beam moves to its next dwelling point, these detectors count the number of interactions and display a pixel on a screen whose intensity is determined by this number. Generally, the more reactions, the brighter the pixel. This process is repeated until the grid scan is finished, and then repeated.

1.7 Objectives of the research

1.7.1 To fabricate the water-stable electrospun polyacrylic acid fiber

1.7.2 To fabricate the LR-SPR sensor chip based on the obtained water-stable electrospun polyacrylic acid fibers

1.7.3 To construct the LR-SPR immunosensor based on the obtained water-stable electrospun polyacrylic acid fibers

1.7.4 To study the sensing property of LR-SPR immunosensor

CHAPTER 2

Experimental Details

2.1 Chemicals and Instruments

2.1.1 Chemicals

All chemicals used in this research are shown in Table 2.1

Table 2.1 Chemicals, Molecular weight, Purity and Company.

Chemical	Purity	Molecular formula	Molecular Weight	Company
Polyacrylic acid (PAA)	98%	$(C_3H_4O_2)_n$	~450000	Sigma-Aldrich
Poly(diallydimethylammonium chloride) (PDADMAC)	97%	$(C_8H_{16}ClN)_n$	~20000 –350000	Sigma-Aldrich
3-Mercapto-1-propanesulfonic acid sodium salt (MPS)	90%	$C_3H_7S_2O_3Na$	178.21	Sigma-Aldrich
β-cyclodextrin	97%	$C_{42}H_{70}O_{35}$	1134.98	Sigma-Aldrich
Phosphate buffered saline, tablet	-	-	-	Sigma-Aldrich
1-Ethyl-3-(3-dimethylamino propyl)-carbodiimide hydrochloride (EDC)	≥98%	$C_8H_{17}N_3$	191.70	TCI MARK
N-Hydroxysuccinimide (NHS)	98%	$C_4H_5NO_3$	115.09	TCI MARK

Table 2.1 (Continued)

Chemical	Purity	Molecular formula	Molecular Weight	Company
Ethanolamine hydrochloride (EA-HCl)	≥99.0%	C_2H_7NO	97.54	TCI MARK
Monoclonal anti-human IgG (Fab specific) produced in goats (Anti-IgG)	-	-	-	Sigma-aldrich
IgG from human serum (IgG)	reagent grade	-	-	Sigma-aldrich

2.1.2 Instruments

The instruments used in the research are summarized in Table 2.2.

Table 2.2 Instrument used in the experiments.

Instrument	Company
Surface plasmon resonance (SPR) spectroscopy instrument	a homemade-attenuated total reflection (ATR) setup using Kretschmann optical configuration
Scanning electron microscopy	-

2.2 SPR and LR-SPR instruments

The attenuated total reflection (ATR) setup used for the excitation of surface plasmons in the classical Kretschmann configuration is shown in Figure 2.1. Surface plasmons are excited by He-Ne laser with λ = 632.8 nm The 2 dielectric layers with similar refractive indices on the opposite side of thin metal film are required in LR-SPR as shown in Figure 2.1(a). The LR-SPR sensor chip which consists of Cytop with refractive index of 1.34 (similar to water with refractive index of 1.33) is spin-coated on the high refractive index glass substrate. The 30 nm of gold film is then deposited by vacuum evaporation on the Cytop film. Figure 2.1(b) is the schematic of conventional SPR sensor chip, the gold film with thickness about 47 nm is deposited on high refractive index glass substrate for optimum excitation of surface plasmons. For both chips, a 2-nm chromium layer is deposited to promote gold adhesion before gold layer deposition.

For demonstration that LR-SPR sensor could be created with multilayer films, the angular scan measurements were performed in ATR setup compared with conventional SPR.

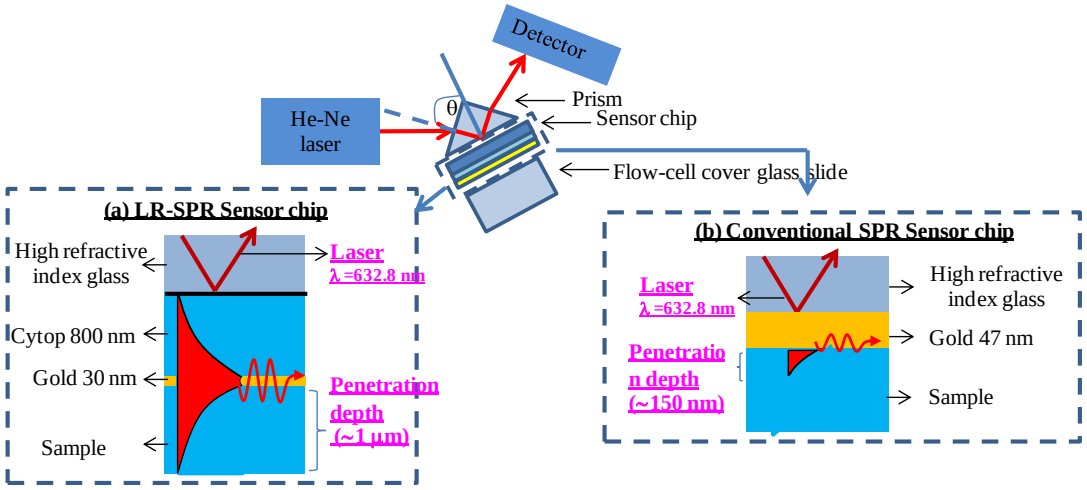

Figure 2.1 Schematic of instrument setup and sensor chip/prism of (a) LR-SPR and (b) conventional SPR at the gold-water interface. [102]

2.3 LR-SPR substrate fabrication

A high refractive index glass slide was employed as a substrate and cleaned before use. The substrate was cleaned in sonication bath in detergent for 15 min followed by deionized (D.I.) water for 15 min and then washed several times with D.I. water. The substrate was then dried in oven about 20–30 minutes.

The dielectric buffer layer was made using Cytop. A 7% Cytop solution (5 g of 9% Cytop, CTL-809M; M-grade was dissolved in 1.45 g Cytop solvent, CTL-180 solvent) was spin-coated on the cleaned glass substrate as shown in Figure 2.2. The Cytop thickness was 800 nm which obtained using an initial spin rate of 500 rpm for 10s which following by 1300 rpm for 20s. The Cytop solvent was removed in an oven

at 180 °C for 1h. The 30 nm gold film was then deposited onto the obtained Cytop-coated glass substrate by vacuum evaporation.

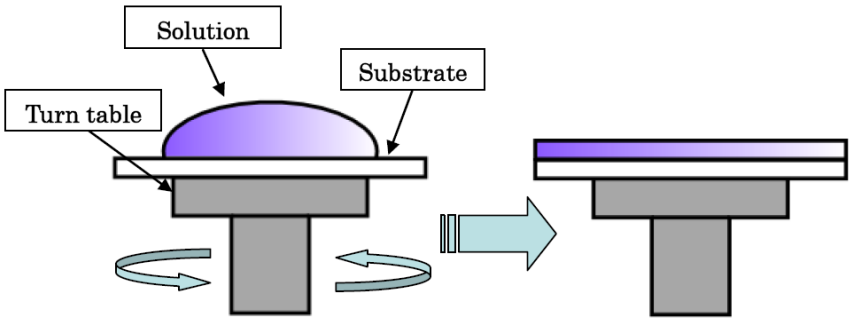

Figure 2.2 Spin-coating of 7% Cytop solution on high-refractive index glass.

Vacuum evaporation of gold film can be done by following method. The gold (Au) thin film was evaporated on the cleaned high refractive index glass slide substrate by thermal vacuum evaporation. The thermal evaporation process is shown in Figure 2.3. The vacuum allows vapor particles to directly travel to the target (substrate), where they condense back to a solid state. The 2 nm of chromium (Cr) thin film was firstly evaporated on the substrate for ensure mechanical stability of the Au film on the glass substrate. Then, on the Cr film, the Au thin film with thickness about 30 nm was chosen for optimum excitation of the surface plasmon vacuum evaporated onto the glass substrate.

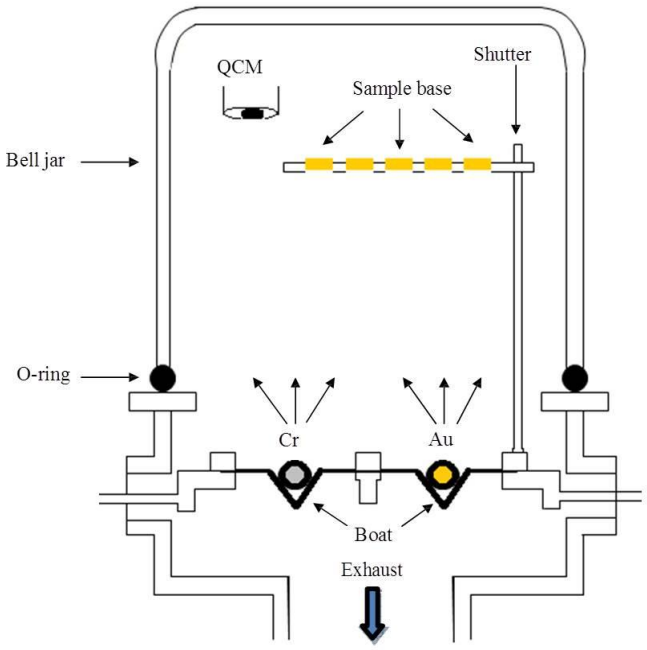

Figure 2.3 Schematic diagram showing vacuum evaporation device [103].

2.4 Fabrication of water-stable electrospun PAA fibers with LbL PAA

Prior to modify an electrospun PAA fiber on the LR-SPR sensor surface, the negative charge of MPS and positive charge of PDADMAC were deposited on the Au film for ensure that the PAA fiber could be deposited on the LR-SPR sensor. The prepared LR-SPR substrate was firstly immersed in 1.0 mM MPS solution (0.178 mg/mL in ethanol) for 180 min to create negatively charge surface, followed by rinsing with D.I water, and then immersed in 1 mg/mL PDADMAC aqueous solution for 15 min to create positively charge surface, respectively. This bilayer could be improved the adhesion of the electrospun PAA fiber.

The electrospinning equipment was setup as shown in Figure 2.4. The β-

cyclodexdrin/PAA fiber (using 0.1 g β-cyclodextrin in 10%wt PAA solution) was then deposited on the surface by electrospinning method with the following condition: the applied voltage of 25 kV, the distance between tip and collector of 15 cm, the diameters of Teflon tube of 1.20 mm and glass pipette of 1.00 mm followed by the crosslinking with annealing at 150 °C for 40 min to increase the water-stability. To further increase the stability of the PAA fibers, the 2 bilayers of positive PDADMAC and negative PAA were then alternately deposited by LbL electrostatic adsorption technique on the surface as shown in Figure 2.6. We therefore called this fiber as "LbL water-stable electrospun PAA fibers" in this study. The schematic of fabrication of the crosslinking PAA is shown in Figure 2.5.

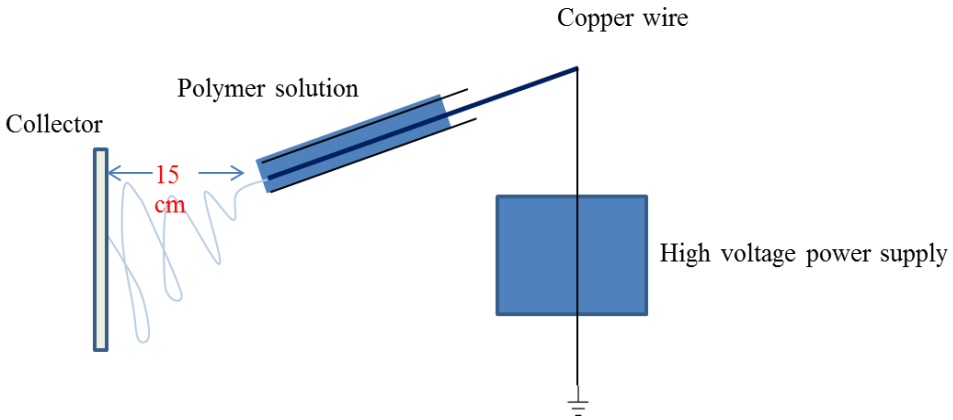

Figure 2.4 The electrospinning equipment setup.

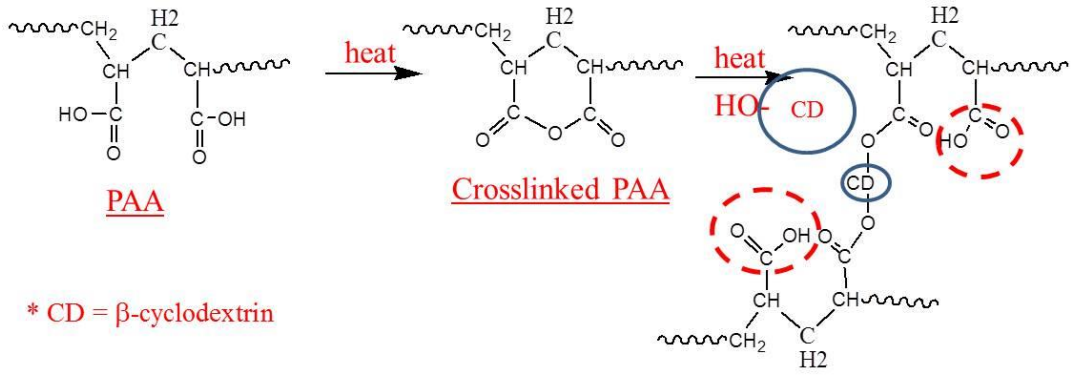

Figure 2.5 Schematic diagram of crosslinking PAA fiber and β-cyclodextrin with thermal treatment [23].

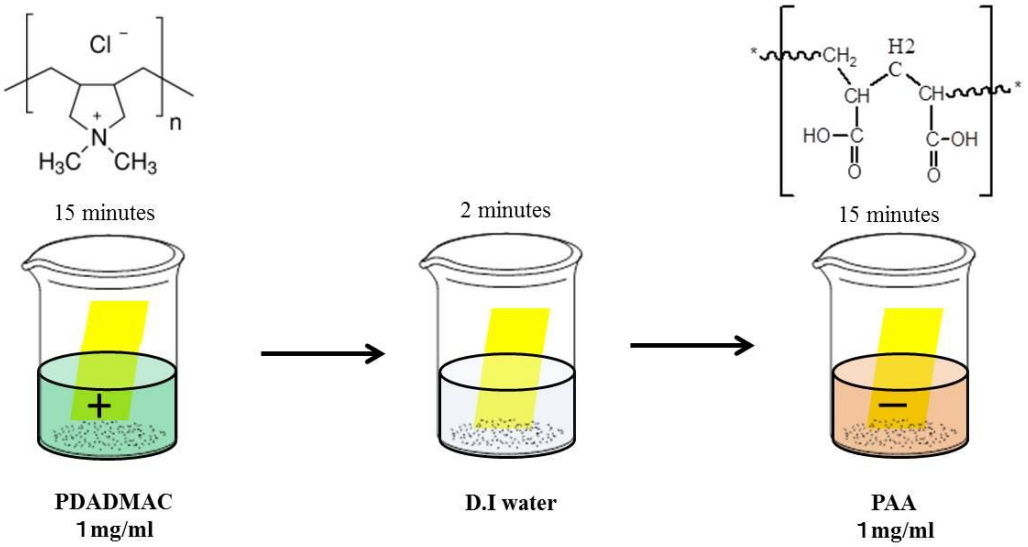

Figure 2.6 LbL of PDADMAC and PAA solution on the substrate.

2.5 Stability of the LbL water-stable electrospun PAA fibers

The stability of the electrospun PAA fibers was studied using angular scan measurements in a classical Kretschman configuration of LR-SPR setup. The angular scan measurements of pure electrospun PAA fibers, crosslinked electrospun PAA fibers, and LbL water-stable electrospun PAA fibers were investigated in water at various times (0 min – 90 min).

2.6 Construction of LbL water-stable electrospun PAA fiber-based immunosensor

The construction of LbL water-stable electrospun fibers based-immunosensor was performed in LR-SPR setup for detection of human IgG. After the LR-SPR baseline was obtained in PBS solution, an aqueous mixture of 0.4 M EDC and 0.1 M NHS (1:1) was injected to activate the carboxylic group of the PAA fibers to *N*-hydroxysuccinimide ester. After rinsing with PBS solution, 100 μg/mL of anti-human IgG was injected for immobilization onto the activated group of the fibers. To deactivate the remaining unreacted *N*-hydroxysuccinimide ester, an aqueous buffer solution of 0.2 M EA-HCl was then injected. The obtained electrospun PAA fibers based-immunosensor was finally employed to detect various concentrations of human IgG.

2.7 Morphology study of the electrospun PAA fibers

The morphology of the obtained electrospun PAA fiber was studied by SEM.

CHAPTER 3

Results and discussion

The comparisons of conventional SPR and LR-SPR sensor chip of the PAA fiber including the properties of the electrospun PAA fiber were studied by using prism coupling surface plasmon resonance spectroscopy. The scanning electron microscopy was also employed to characterize the electrospun PAA fibers.

Prior to fabrication of PAA fiber, the appropriate thickness of Cytop was determined by LR-SPR angular scan measurement. The thickness of the dielectric buffer layer or 7% Cytop was varied from 500 to 900 nm by spin coating the solution on the BK7 substance before evaporation of 30 nm Au film on the top. From Figure 3.1, the dip angle of LR-SPR angular reflectivity curves is lowest at the thickness of 800 nm and the width of the curve is decreased which indicated that the optimum Cytop thickness for this study is 800 nm because the electric field intensity will be highest with maximum coupling of the incident light.

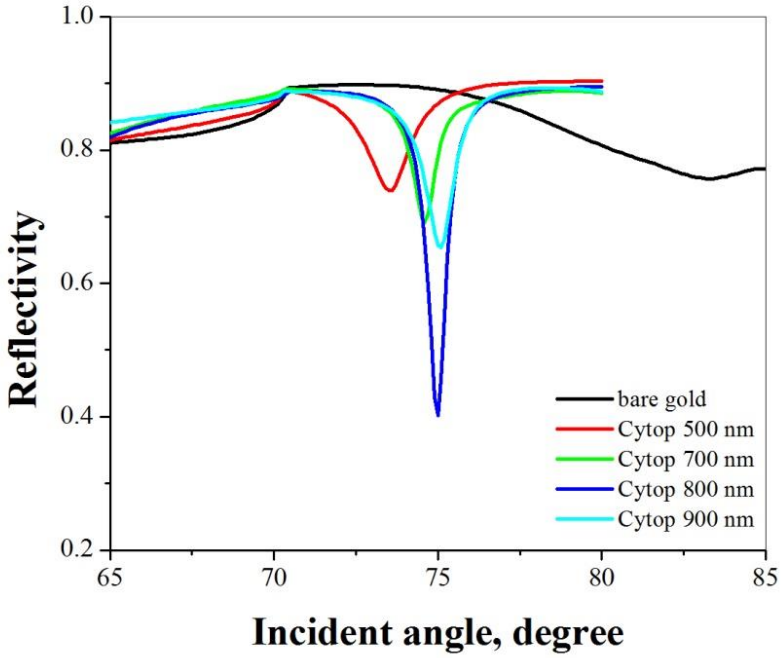

Figure 3.1 LR-SPR angular reflectivity scan curves of the various thickness of Cytop layer on Au film.

3.1 Comparison of angular-reflectivity curve between conventional-SPR and LR-SPR setup

A typical angular-reflectivity curve is demonstrated in the reflectivity versus incident angle on the prism. The reflectivity starts from a value below 1.0 and increase to a reflectivity close to 1.0 which the angle at this reflectivity is called “critical angle”. The reflectivity stays more or less constant and starts to decrease until a minimum value close to zero is reached. With increasing incident angle, the intensity recovers in a slightly asymmetric form. The decreasing in the reflectivity curve is called “surface plasmon”. The resonance angle is located in the minimum reflectivity. By adding other

layers to the thin metal film, the resonance of the surface plasmon shifts to a higher angle [57]. Comparison of the angular-reflectivity curves between the conventional SPR and LR-SPR sensor chips showed different in dip angle positions which the resonance curve of the LR-SPR chip is much sharper with more symmetric shape than conventional SPR chip as shown in Figure 3.2. The LR-SPR curve is occurred at the lower angle with a narrower shape than the conventional SPR. The narrow resonance in the LR-SPR angular-reflectivity curve is associated with the excitation of LR-SPR mode at the gold-water interface. Moreover, the dip angle is part of an interference pattern which fringe spacing is dependent on the thickness of the Cytop layer [57].

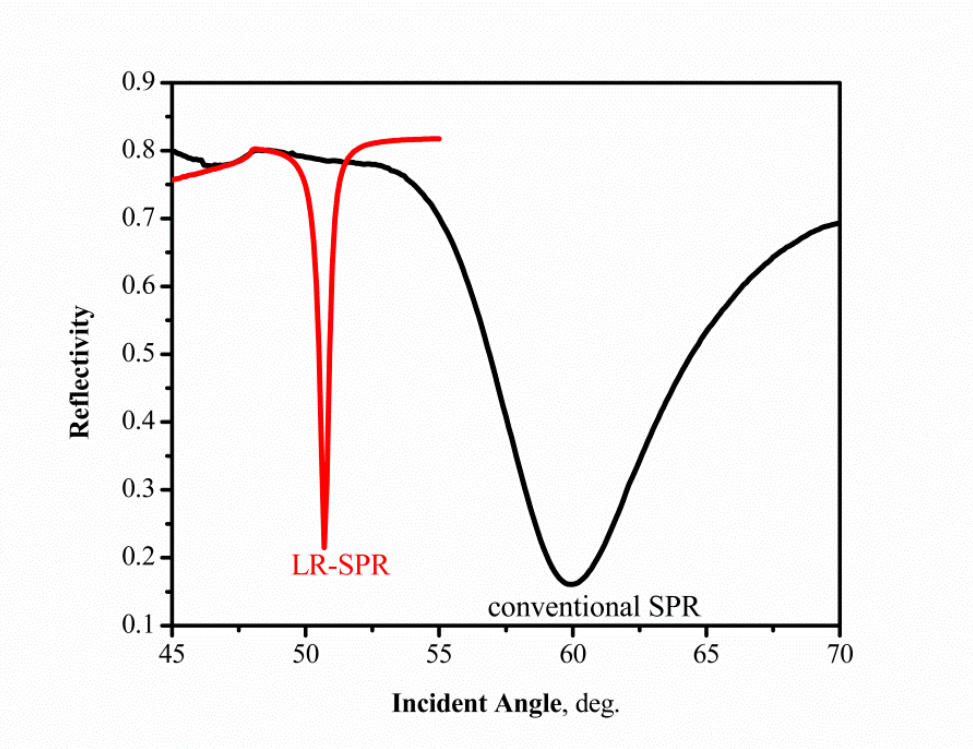

Figure 3.2 Conventional SPR and LR-SPR angular reflectivity curves.

3.2 Fabrication of water-stable electrospun PAA fibers with LbL-PAA fiber

The pure PAA fiber can be solubilized in aqueous solution, therefore, we have tried to develop the crosslinked PAA by adding β-cyclodextrin for construction of immunosensor in this research. The higher concentration of β-cyclodextrin made the larger size of fiber due to the β-cyclodextrin cannot completely dissolve which led the fiber to be a bead. Moreover, if the ratio of water : ethanol is high, the viscosity of PAA solution is low. This leads to a non-continuous fiber. Therefore, the electrospun PAA fibers were fabricated using PAA solution in 4:1 water : ethanol with 10% β-cyclodextrin added into the glass pipet with 0.1 mm inner-diameter and Teflon tube with 1.2 mm inner-diameter followed by heat treatment at 180 °C for 40 min. The electrospinning setup is shown in Figure 2.4. The obtained electrospun PAA fibers were characterized by scanning electron microscopy (SEM). The SEM images are shown in Figure 3.3. The average diameter of the electrospun PAA fiber from the glass pipet was 0.475 μm as can be obtained from Figure 3.3(a) whereas the diameter of the electrospun PAA fiber from Teflon tube was 0.671 μm as can be obtained from Figure 3.3(b). The electrospun PAA fiber from glass pipet was chosen and used in the LR-SPR experimental due to its thinner and smoother than the fiber from Teflon tube.

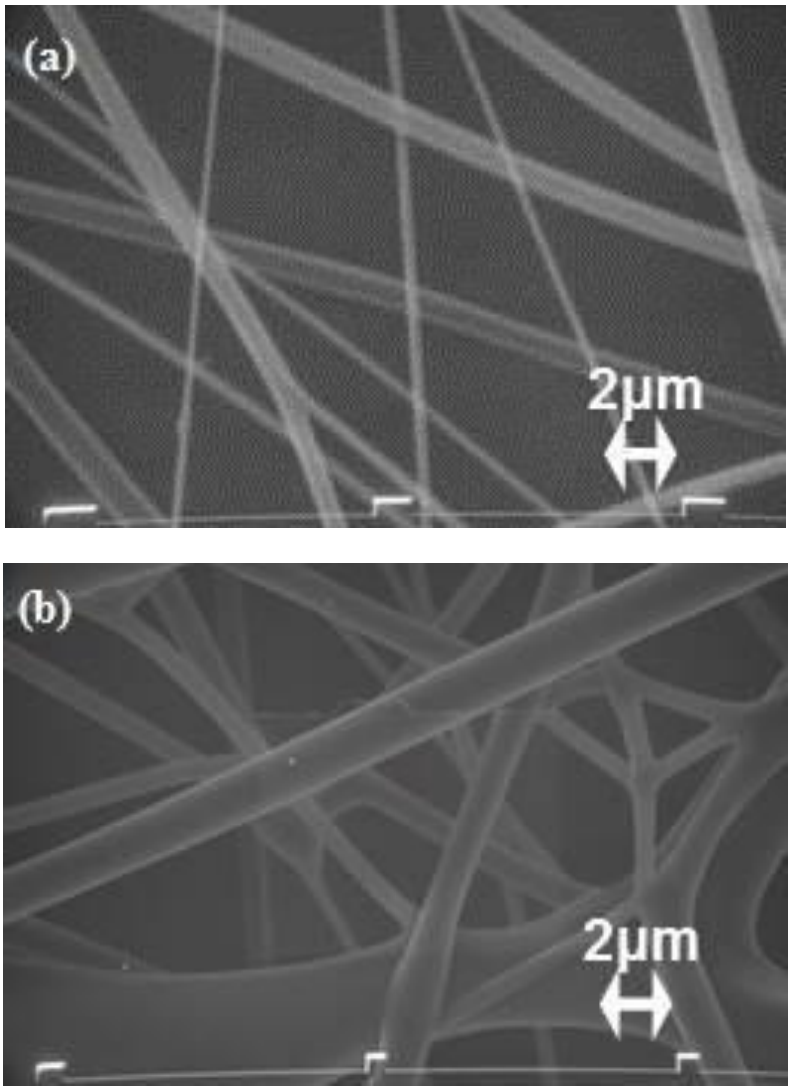

Figure 3.3 SEM images of electrospun PAA fibers after heat treatment from (a) glass pipet (b) Teflon tube.

The structure of electrospun PAA fibers in this work is shown in Figure 3.4. Due to completely dissolving of the pure PAA fiber, the crosslinked electrospun PAA fiber was produced by adding β-cyclodextrin as crosslinker followed by thermal treatment. The dehydration of carboxylic groups of PAA was occurred followed by esterification with hydroxyl groups of β-cyclodextrin during thermal treatment [23]. This led the crosslinked electrospun PAA fiber contained less number of carboxylic groups in the polymer chain compared to the pure PAA fiber. However, a numerous of carboxylic groups of the polymer surface are useful in biosensor and immunosensor applications. We, therefore, employed LbL deposition technique to increase the number of the carboxylic groups and stability of the fibers in this study. The LbL deposition technique involves the alternate adsorption of anionic and cationic polyelectrolytes on a charged substrate of MPS by subsequently dipping the substrate into the aqueous polyelectrolyte solutions which becomes a thin polymer film on the substrate [90–92, 98]. In this present work, the crosslinked electrospun PAA fibers with negative charge on the surface were coated by alternated LbL multilayers deposition of positive PDADMAC and negative PAA for 3 bilayers, thus leaving the high surface area of the electrospun fibers and increased the carboxylic groups of PAA surface [23]. We therefore called these fibers as “LbL water-stable electrospun PAA fibers” in this study. The schematic view of LR-SPR chip after surface improvement by LBL deposition of positive PDADMAC and negative PAA is shown in Figure 3.4.

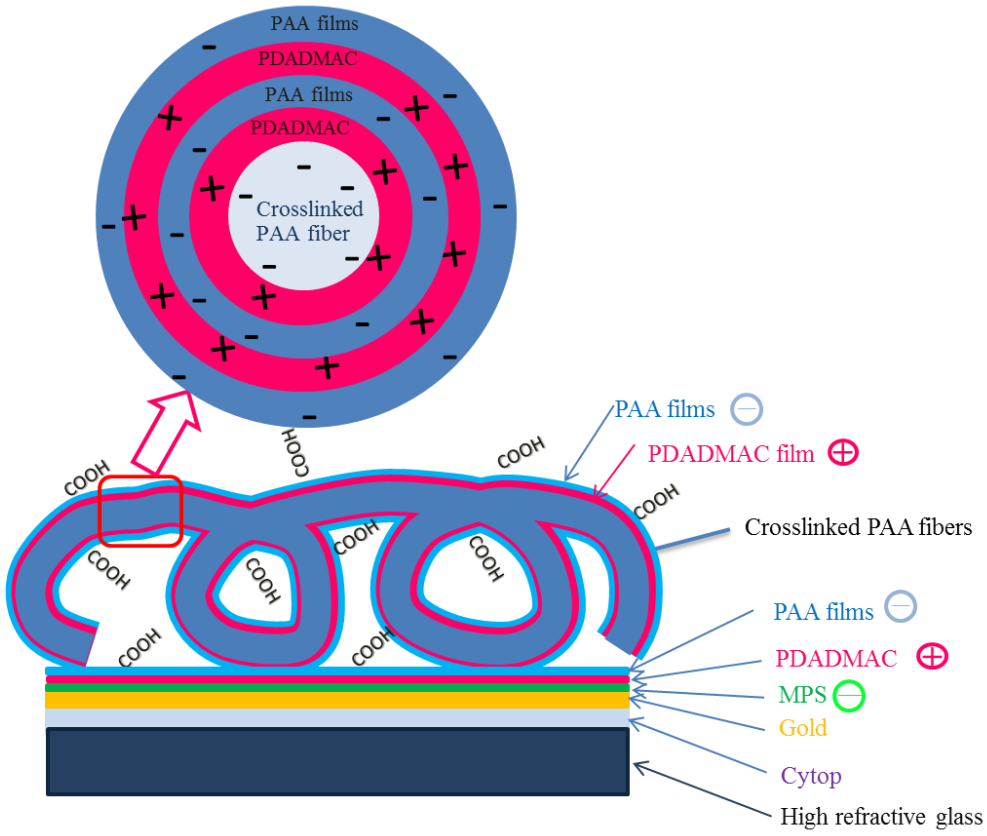

Figure 3.4 Schematic view of LR-SPR chip after surface improvement by LBL deposition of positive PDADMAC and negative PAA.

In addition, the conventional SPR and LR-SPR sensor chip are compared by monitoring the angular scan curves of 1 bilayer LbL crosslinked-electrospun PAA fibers as shown in Figure 3.5. The different of both sensor chips is the Cytop layer between glass slide and gold layer in LR-SPR sensor chip. After electrospinning of crosslinked electrospun PAA fibers on both conventional and LR-SPR sensor chips, the electrospun PAA fiber chip was then mounted to SPR Teflon cell. The LbL deposition process was mainly carried out in the following 2 steps: (1) PDADMAC solution was

firstly injected in SPR Teflon cell for 15 min and subsequently washed with D.I. water for 2 min and (2) after washing step, PAA solution was then injected for 15 min, followed by washing with D.I. water. The angular-reflectivity scan was then performed. The thickness of the LbL crosslinked-electrospun PAA fibers was assumed to be equal in both sensor chips. The LR-SPR resonance angle, was shifted to higher angle (Figure 3.5b) while the conventional SPR dip angle was shifted to lower angle (Figure 3.5a). It indicated that LR-SPR sensor chip has larger penetration depth of the evanescent wave which shows more sensitivity compared to conventional SPR [57].

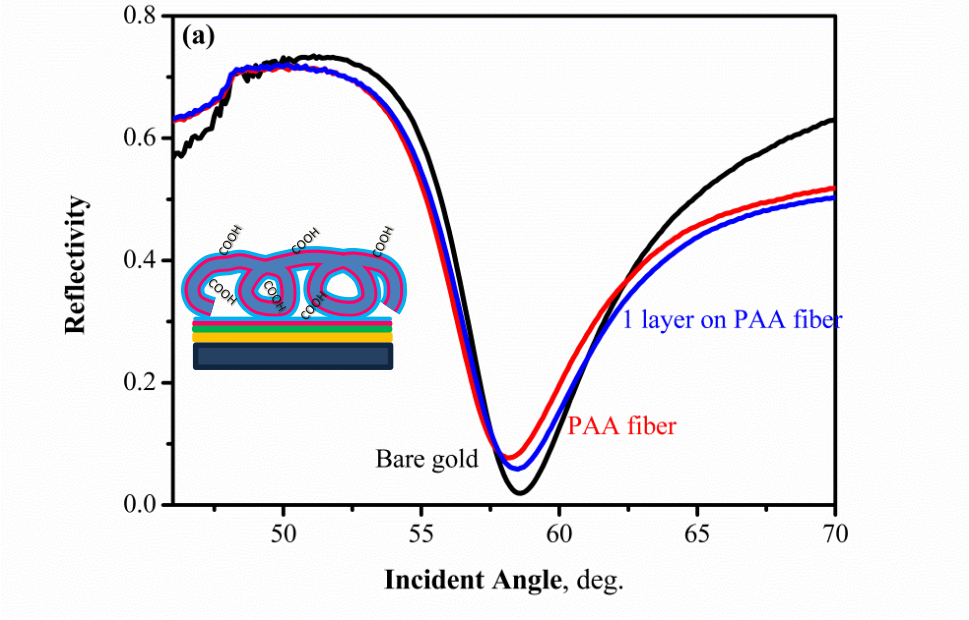
(a)
Reflectivity
0.8
0.6
0.4
0.2
0.0
50
55
60
65
70
Incident Angle, deg.
COOH
1 layer on PAA fiber
PAA fiber
Bare gold

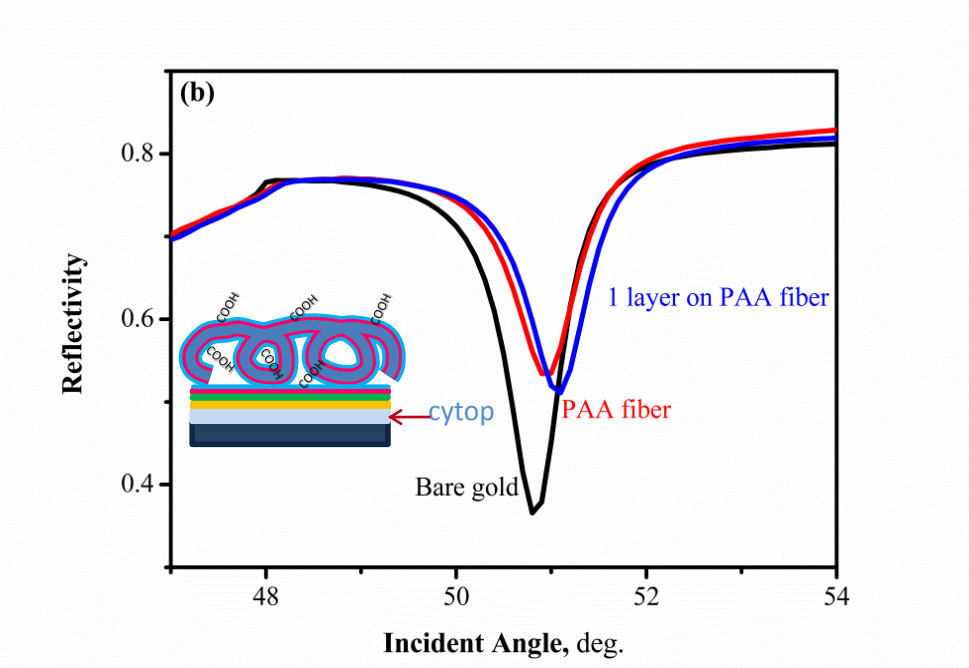
(b)
Reflectivity
0.8
0.6
0.4
48
50
52
54
Incident Angle, deg.
COOH
1 layer on PAA fiber
cytop
PAA fiber
Bare gold

Figure 3.5 Angular-reflectivity curves of electrospun PAA fiber in water after LbL deposition of PDADMAC and PAA for 1 bilayer of (a) conventional SPR and (b) LR-SPR.

3.3 Stability of the LbL water-stable electrospun PAA fibers

Since the pure PAA fiber is water soluble material, we therefore improved the stability of the PAA fiber by crosslinking with β-cyclodextrin. The water-stable of PAA fibers were produced to retain their fiber structure by adding β-cyclodextrin as crosslinking agent into an aqueous PAA solution and then heated at 150 °C for 40 min. The structure of crosslinked PAA fibers was earlier reported elsewhere [23]. These electrospun PAA fibers are insoluble in water. Moreover, for further increasing the stability of the crosslinked PAA fibers, the 3 bilayers of positively PDADMAC and negatively PAA were alternately deposited by LBL technique on the PAA fibers. The stability of the fibers in water was studied by measuring the LR-SPR angular-reflectivity curves of the fibers in water at various soaking times as seen in Figure 3.6. The LR-SPR reflectivity curves of all fibers were shifted to high angle compared with bare gold. However, the PAA fibers were disappeared from the gold substrate surface after 20 min as can be seen from the dip angle of LR-SPR reflectivity curve in Figure 3.6(a) was shifted to lower angle and return back to the same position with the bare gold. This indicated that the electrospun PAA fibers completely dissolved in water. Stability of the crosslinked PAA fibers is shown in Figure 3.6(b). Shift of the dip angle was slightly observed indicating a small amount of the fibers had been peeled off after soaking in water for several minutes. The interesting result was observed for the LbL water-stable electrospun PAA fibers as shown in Figure 3.6(c). The dip angle was still

at the same position even after soaking the fibers for 90 min in water. This indicates that the LbL water-stable electrospun PAA fibers show the most stable in this study. The dip angle of the LbL water-stable electrospun PAA fibers was higher and broader than that of the crosslinked PAA fibers (before LbL) which refers to the more PAA alternated with PDADMAC and that more carboxylic group on the fiber surface. We therefore decided to use this LbL water-stable electrospun PAA fiber as sensor chip for construction of immunosensor.

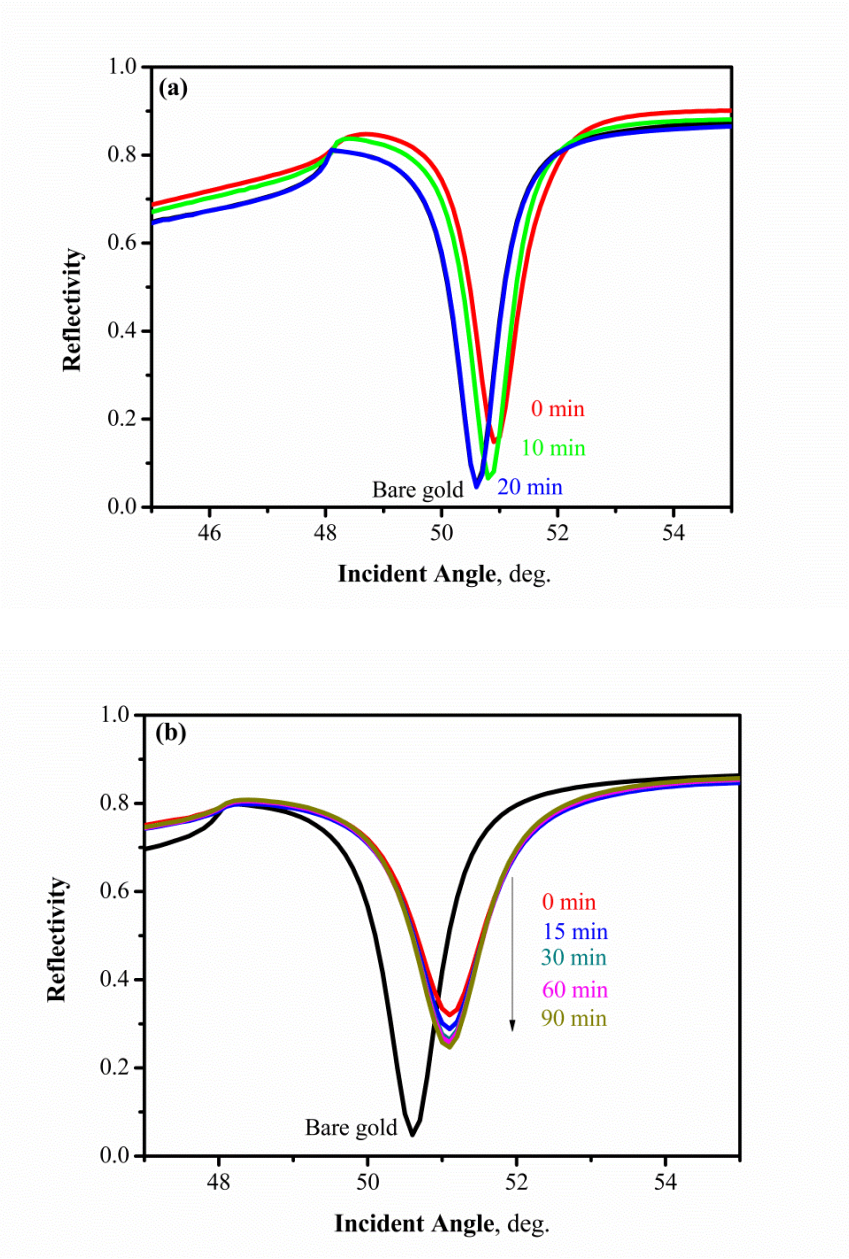

Figure 3.6 LR-SPR angular reflectivity curves of (a) PAA fibers (b) crosslinked PAA fibers and (c) LbL water-stable electrospun PAA fibers.

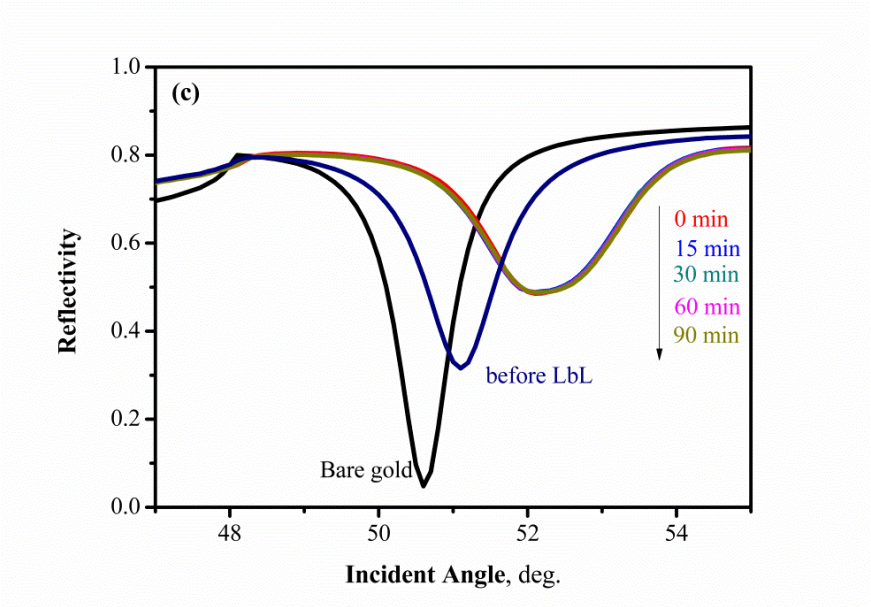

Figure 3.6 continued.

For further study the advantage of the fibers on LR-SPR sensor chips, the LbL on the substrate without electrospun PAA fiber surface was chosen to compare with the LbL on the water-stable electrospun PAA fiber. The LR-SPR angular scan curves are shown in Figure 3.7. Shift of the resonance dip angle was obviously observed for the LbL on the water-stable electrospun PAA fiber as shown in Figure 3.7(b) comparing with slightly change in the LbL without fiber surface as shown in Figure 3.7(a). This obvious change indicates the advantage of the water-stable electrospun PAA fiber for use as LR-SPR immunosensor.

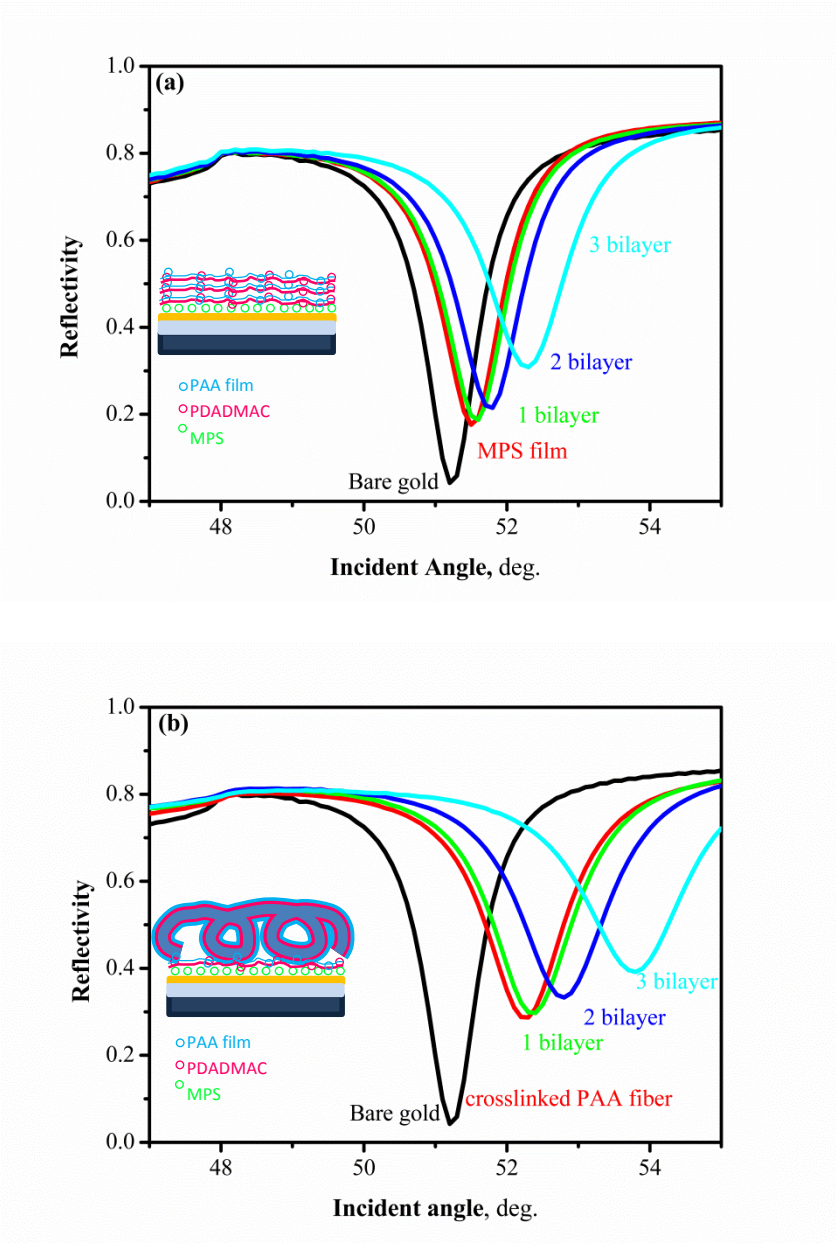

Figure 3.7 LR-SPR angular reflectivity curves of PDADMAC/PAA LbL bilayers (a) without electrospun PAA fiber (b) on electrospun PAA fiber.

3.4 Construction of electrospun PAA fiber-based immunosensor

The LR-SPR chip, as shown in Figure 3.4, was then employed for construction of immunosensor for detection of human IgG at various concentrations. The sensing property of electrospun PAA fiber was studied by immobilizing anti-human IgG on carboxylated electrospun PAA fiber through covalent bond. The real time monitoring was performed using SPR kinetic measurement during construction of the electrospun PAA fiber based immunosensor as shown in Figure 3.8. The EDC/NHS coupling reagent was employed to activate the carboxylic group of PAA fibers to NHS-ester group. After rinsing the fiber with PBS, the 100 μg/mL anti-human IgG was injected and immobilized to the activated group on the surface. The reflectivity increased during the immobilization process indicating the binding of anti-human IgG on the fiber surface. A non-immobilized surface of the activation group was then deactivated by EA-HCl buffer solution before detection of human IgG.

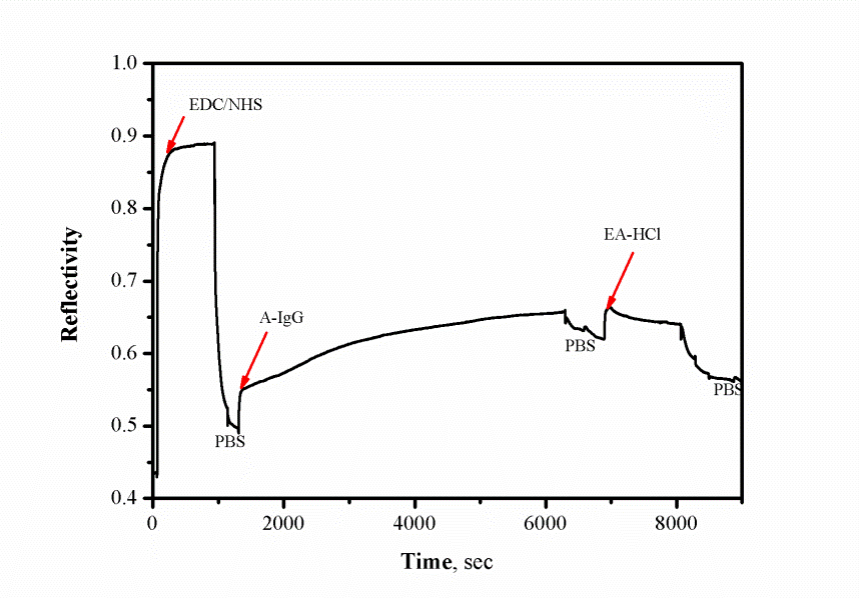

Figure 3.8 SPR kinetic curve during construction of the LbL water-stable electrospun PAA fiber-based immunosensor.

The construction of immunosensors using the LbL film on bare surface and LbL on crosslinked PAA fibers as LR-SPR sensor chips were investigated by LR-SPR spectroscopy. The LR-SPR angular reflectivity curves during construction of the immunosensors for detection of human IgG (sensing) on both sensor chips are shown in Figure 3.9. The resonance dip angles after immobilization of anti-human IgG and detection of human IgG on LbL crosslinked-electrospun PAA fiber sensor chips (Figure 3.9(b)) were obviously shifted to higher angles comparing with the dip angles of LbL on bare surface sensor chips (Figure 3.9(a)). This can be confirmed that LbL crosslinked electrospun PAA fibers can adsorb more amount of anti-human IgG on fiber due to the more surface area and carboxylic group on the sensor chip surface. Therefore, it can be concluded that the LR-SPR sensor chip with LbL crosslinked electrospun PAA fiber exhibited more sensitivity.

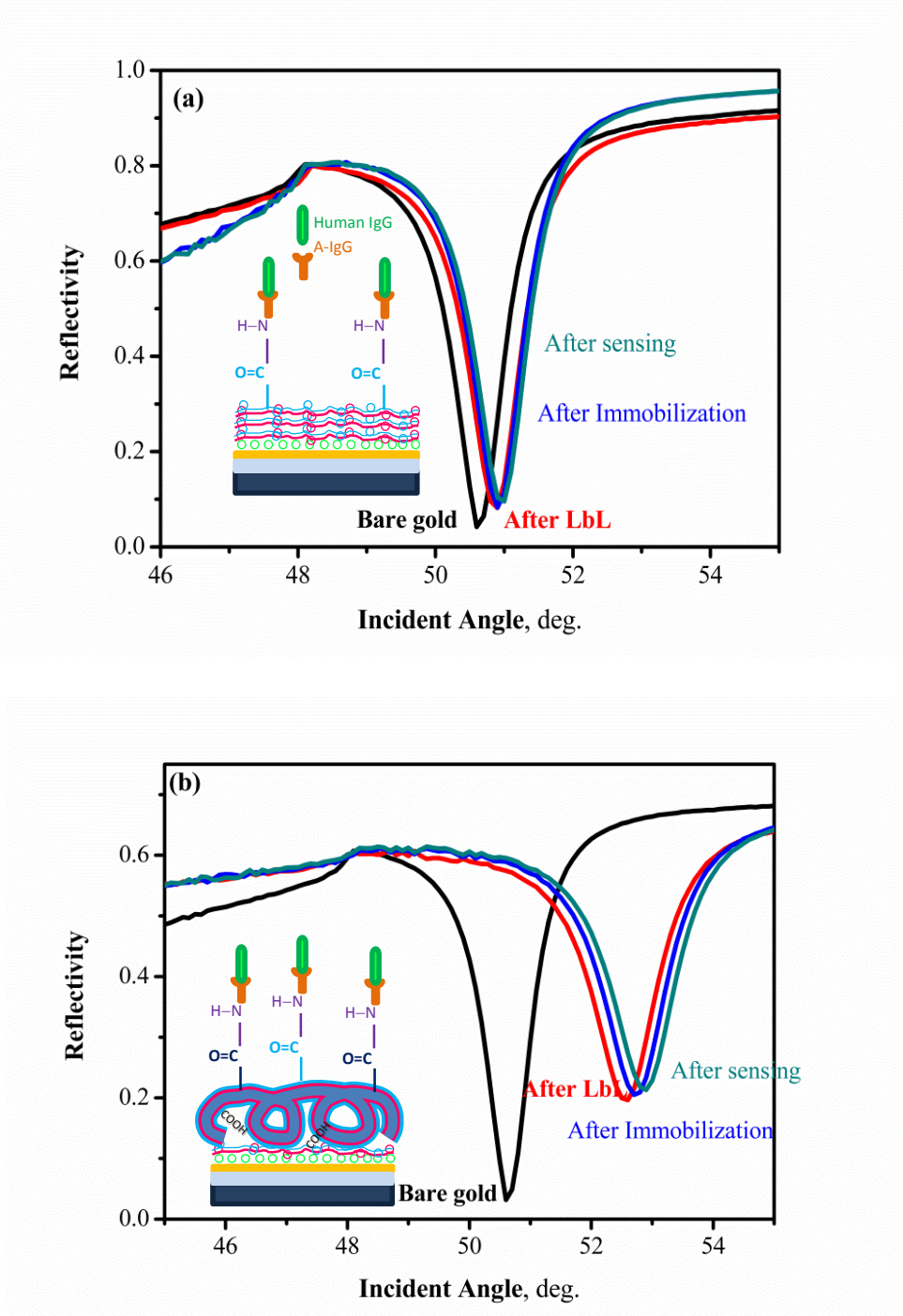

Figure 3.9 SPR angular reflectivity curve during the construction of immunosensor for the binding of human IgG on (a) 1 bilayer LbL on bare surface (b) 1 bilayer LbL crosslinked-electrospun PAA fibers.

Finally, the constructed LR-SPR immunosensor based on water-stable PAA fibers was employed for detection of human IgG (at concentrations of 1, 5, 10 μg/mL in PBS buffer solution). The dip angles before and after human IgG sensing processes were measured. Table 3.1 shows the dip angle reflectivity changes after sensing with human IgG. The reflectivity change was increased with the concentrations of human IgG. This can be confirmed that the LR-SPR immunosensor based on water-stable PAA fibers can be used for detection of human IgG.

Table 3.1 Dip angle reflectivity change after sensing with human IgG.

Concentration of human IgG (μg/mL)	Reflectivity change
1	0.0078
5	0.2262
10	0.2520

CHAPTER 4

Conclusions

In this study, the water-stable electrospun polyacrylic acid (PAA) fibers were successfully fabricated by adding β-cyclodextrin as crosslinking agent followed by thermal treatment at 180 °C for 40 min after electrospinning process due to its stability in the aqueous solution. The dip angle of the non-crosslinking fiber was changed due to its peel off from the substrate which indicated the unstable fiber. The water-stability and sensitivity of the fibers were improved using layer-by-layer (LbL) alternate deposition of anionic PAA and cationic poly(diallyldimentylammonium chloride) (PDADMAC) polyelectrolyte solutions. The LbL of PAA and PDADMAC was successfully prepared. In angular scan measurement, the dip angle of LR-SPR reflectivity of the fiber after incubate in aqueous solution for 90 min was not changed which indicating that this obtained LbL crosslinking electrospun fiber was very stable in the aqueous solution and contained more amount of available carboxyl groups which necessary for adsorption the biomolecule. Comparison of the angular scan measurement of the LbL water-stable electrospun fiber with flat MPS surface (the gold substrate after charged with MPS), the dip angle was shifted to higher angle due to the LbL of the fiber. In biosensing study, the reflectivity was increased after injection of each chemical due to the binding process which occurred on the sensor chip. By increasing the concentration of human-IgG, the dip angle in angular scan measurement was changed to higher angle, indicating that this LR-SPR sensor chip has a concentration-dependent and can be used to detect human IgG.

The LbL crosslinked-electrospun PAA fibers can be employed as LR-SPR sensor chip which consists of thin gold film and layer of Cytop. The LR-SPR sensor has larger evanescent field intensity and penetration depth as compared to conventional SPR. Since the LbL crosslinked-electrospun PAA fibers can enhance the signal of LR-SPR spectroscopy, therefore, the water-stable electrospun PAA fibers based LR-SPR immunosensor was successfully constructed for detection of human IgG. The LR-SPR sensor chip based on the water-stable PAA fiber can be used as a biosensor in the further work which more further experiments would be performed.

REFERENCE

[1] Thevenot DR, Toth K, Durst R.A, Wilson G.S, Electrochemical Biosensors: Recommended Definitions and Classification, *Pure Appl. Chem*., **7**, 1999, 2333–2348.

[2] Clark, L.C., Lyons, C., Ann N. Y., Electrode systems for continuous monitoring cardiovascular surgery, *Acad. Sci*., **102**, 1962, 29–45.

[3] Habib, M. K., Controlled biological and biomimetic systems for landmine detection, *Biosens. Bioelectron.*, **23**, 2007, 1–18.

[4] Nguyen-Boisse, T.T., Saulnier, J., Jaffrezic-Renault, N., Lagarde, F., Highly sensitive conductometric biosensors for total lactate, d- and l-lactate determination in dairy products, *Sens. Actuators B Chem.*, **179**, 2013, 232–239.

[5] Nouira, W., Maaref, A., Elaissari, H., Vocanson, F., Siadat, M., Jaffrezic-Renault, N., Comparative study of conductometric glucose biosensor based on gold and on magnetic nanoparticles, *Mater. Sci. Eng. C.*, **33**, 2013, 298–303.

[6] Lakard, B., Magnin, D., Deschaume, O., Banlancker, G., Glinel, K., Demoustier-Chamagne, S., Nysten, B., Jonas, A.M., Bertrand, P., Urea potentiometric biosensor based on charged biopolymers and electrodeposited polyaniline, *Biosens. Bioelectro*n., **26**, 2011, 4139–4145.

[7] Ameer, Q., Adeloju, S. B., Development of a potentiometric catechol biosensor by entrapment of tyrosinase within popyrrole film, *Sens. Actuators B Chem*., **140**, 2009, 5–11.

[8] Batra, B. Lata, S., Sharma, M., Pundir, C. S., An acrylamide biosensor based on immobilization of hemoglobin onto multiwalled carbon nanotube/copper nanoparticles/polyaniline hybrid film, *Anal. Biochem.*, **433**, 2013, 210–217.

[9] Soylemez, S., Kanik, F. E., Ileri, M., Hacioglu, S. O., Toppare, L., Development of a novel biosensor based on a conducting polymer, *Talanta*, **118**, 2014, 84–89.

[10] Prasad, B.B., Pandey, I., Molecular imprinted polymer-based piezoelectric sensor for enantio-selective analysis of malic acid isomers, *Sens. Actuators B Chem.*, **181**, 2013, 596–604.

[11] Lu, H. H., Rao, Y. K., Wu, T. Z., Tzeng, Y. M., Direct characterization and quantification of volatile organic compounds by piezoelectric module chips sensor, *Sens. Actuators B Chem.*, **137**, 2009, 741–746.

[12] Fan, X., White, I. M., Shopova, S. I., Zhu, H., Suter, J. D., Sun, Y., Sensitive optical biosensors for unlabeled targets: A review, *Anal. Chim. Acta*, **620**, 2008, 8–26.

[13] Long, F., Zhu, A., Shi, H., Recent advances in optical biosensors for environmental monitoring and early warning, *Sensors*, **13**, 2013, 13928–13948.

[14] Doshi, J., Reneker, D. H., Electrospinning process and applications of electrospun fibers, *J. Electrostat.*, **35**, 1995, 151–160.

[15] Gupta, P., Casey, E., Timothy, E. L., Wilkes, G. L., Electrospinning of linear homopolymers of poly(methyl methacrylate): exploring relationships between fiber formation, viscosity, molecular weight and concentration in a good solvent, *Polymer*, **46**, 2005, 4799–4810.

[16] Han, S. O., Youk, J. H., Min, K., D., Kang, Y. O., Park W. H., Electrospining of cellulose acetate nanofibers using a mixed solvent of acetic acid/water: effects of solvent composition on the fiber diameter, *Materials letters*, **62**, 2008, 759–762.

[17] Thompson, C. J., Chase, G. G., Yarin, A. L., Reneker, D. H., Effects of parameters on nanofiber diameter determined from electrospinning model, *Polymer*, **48**, 2007, 6913–6922.

[18] Chowdhury, M., Stylios, G., Effect of experimental parameters on the morphology of electospun nylon 6 fibres, *International J. Basic & Applied Sciences IJBAS-IJENS*, **10**, 2010, 70–78.

[19] Homayoni, H., Ravandi, S. A. H., Balizadeh, M., Electrospinning of chitosan nanofibres: processing optimization, *Carbohydrate Polym.*, **77**, 2009, 656–661.

[20] David, F. C., Electrospinning[online]. Available from: http://www.che.vt.edu/wilkes/electrospinning/electrospinning.htmil. [2009, October 4]

[21] Tan, S.-H, Inai, R., Kotaki, M., Ramakrishna, S., Systematic parameter study for ultra-fine fiber fabrication via electrospinning process, *Polymer*, **46**., 2005, 6128 –6134.

[22] Ramakrishna, S.; Fujuhara, K. An introduction to electrospinning and nanofibers, World Scientific Publishing: Singapore, 2005.

[23] Li, L.; Hsieh,Y. L. Ultra-fine polyelectrolyte fibers form electrospinning of poly(acrylic acid). *Polymer* **46,** 2005, 5133-5139.

[24] Shinbo, K.; Onozuka, S.; Hoshino, R.; Mizuno, Y.; Ohdaira, Y.; Baba, A.; Kato, K.; Kaneko, F. Preparation of electrospun polymer fibers using a copper wire electrode in a capillary tube. *Jpn. J. Appl. Phys*. **49**, 2010, 04DK24-1-04DK24-5.

[25] Doshi, J.; Reneker, D. H. Electrospinning process and applications of electrospun fibers. *J. Electrostat.*, **35**, 1995, 151-160.

[26] Beachley, V.; Wen, X. Effect of electrospinning parameters on the nanofiber diameter and length. *Mat. Sci. Eng. C.,* **29**, 2009, 663-668.

[27] Li, M.; Guo, Y.; Wei, Y.; MacDiarmid, A. G.; Lelkes, P. I. Electrospinning Polyaniline-contained gelatin nanofibers for tissue engineering applications. *Biomaterials*, **27**, 2006, 705-2715.

[28] Meng, Z. X.; Xu, X. X.; Zheng, W.; Zhou, H. M.; Li. L.; Zheng, Y. F.; Lou, X. Preparation and characterization of electrospun PLGA/gelatin nanofibers as potential drug delivery system. *Colloids Surf., B: Biointerfaces*, **84**, 2011, 97-102.

[29] Li, D.; Frey, M. W.; Baeumner, A. J. Electrospun polylactic acid nanofiber membranes as substrates for biosensor assemblies. *J. Memb. Sci.*, **279**, 2006, *279*, 354-363.

[30] Pyun, J. C.; Beutel, H.; Meyer, J,-U.; Ruf, H. H. Development of a biosensor for E.coli based on aflexural plate wave (FPW) transducer. *Biosens. Bioelectron*. **13**, 1998, 839-845.

[31] Wang, X.; Drew, C.; Lee, S. H.; Senecal, K. J.; Kumar, J.; Samuelson, L.A. Electrospinning technology: A novel approach to sensor application., *J. of Macromol. Sci*. **A39**, 2002, 1251-1258.

[32] Bhardwaj, N.; Kundu, S. C. Electrospinning: a fascinating fiber fabrication technique. *Biotechnol. Adv*., **28**, 2010, 325-347.

[33] Aussawasathien, D.; Dong, J. -H.; Dai, L. Electrospun polymer nanofiber sensors. *Synth. Met*., **154**, 2005, 37-40.

[34] Luo, Y.; Nartker, S.; Miller, H.; Hochhalter, D.; Wiederoder, M.; Wiederoder, S.; Setterington, E.; Drzal, L. T.; Alocilja, E. C. Surface functionalization of electrospun nanofibers for detecting E. coli O157:H7 and BVDV cells in a direct-charge transfer biosensor., *Biosens. Bioelectron*., **26**, 2010, 1612-1617.

[35] Ding, B.; Kim, J.; Miyazaki, Y.; Shiratori, S. Electrospun nanofibrous membranes coated quartz crystal microbalance as gas sensor for NH3 detection. *Sens. Actuators B*, **101**, 2004, 373-380.

[36] Homola, J., Yee, S. S., Gauglitz, G., Surface plasmon resonance sensor: review, *Sens. Actuators B Chem.*, **54**, 1999, 3–15.

[37] Geogiadia, R., Peterling, K. P., Peterson, A. W., Quantitative measurements and modeling of kinetics in nucleic acid monolayer films using SPR spectroscopy, *J. Am. Chem. Soc*., **122**, 2000, 3166–3173.

[38] Guedon, P., Livache, T., Martin, F., Lesbre, F., Roget, A., Bidan, G., levy, Y., Characterization and optimization of a real-time, parallel, label-free, polypyrrole-based DNA sensor by surface plasmon resonance imaging, *Anal. Chem*., **72**, 2000, 6033–6009.

[39] Badia, A., Arnold, S, Scheumann, V., Zizlsperger, M., Mack, J., Jung, G., Probing the electrochemical deposition and/or desorption of self-assembled and

electropolymerizable organic thin films by surface plasmon spectroscopy and atomic force microscopy, *Sens. Actuators B Chem.*, **54**, 1999, 145-165.

[40] Iwasaki, Y., Horiuchi, T., Niwa, O., Detection of electrochemical enzymatic reactions by surface plasmon resonance measurement, *Anal. Chem*., **73**, 2001, 1595−1598.

[41] Tsoi, P. Y., Yang, J., Sun, Y. Sui, S., Yang, M., Surface plasmon resonance study of DNA polymerases binding to template/primer DNA duplexes immobilized on supported lipid monolayers, *Langmuir*, **16**, 2000, 6590−6596.

[42] Suzuki, M., Nakashima, Y., Mori, Y., *Sens. Actuators B Chem*., **54**, 1999, 176−181.

[43] Liedberg, B., Nylander, C., Lundstrom, I., Biosensing with surface plasmon resonance-how it all started, *Biosens. Bioelectron*., **10**, 1995, i–ix.

[44] Homola, J., Surface plasmon resonance sensors for detection of chemical and biological species, *Chem. Rev.*, **108,** 2008, 462−493.

[45] Wood, R., On a remarkable case of uneven distribution of light in a diffraction grating spectrum, *Phil. Mag*., **4**, 1902, 396−402.

[46] Ritchie, R., Arakawa, E., Cowan, J., Hamm, R., Surface-plasmon resonance effect in grating diffraction, *Phys. Rev. Lett*., **21**, 1968, 530−1532.

[47] Otto, A., Excitation of surface plasma waves in silver by the method of frustrated total reflection, *Z. Physik*, **216**, 1968, 398−410.

[48] Knoll, W., Interface and thin film as seen by bound electromagnetic waves, *Annu. Rev. Phys. Chem.*, **49**, 1988, 569−638.

[49] Hickel, W., Rothenhausler, B., Knoll, W., Surface plasmon microscopic characterization of external surfaces, *J. Appl. Phys*., **66**, 1989, 4832–4836.

[50] Schasfoort, R. B. M., Tudos, A. J., Handbook of surface plasmon resonance, RSC publishing, Cambrigde, 2008.

[51] Advincula, R. C., Aust, E., Meyer, W., Knoll, W., *In situ* investigations of polymer self-assembly solution adsorption by surface plasmon spectroscopy, *Langmuir*, **12**, 1996, 3536–3540.

[52] Xia, C., Advincula, R. C., Baba, A., Knoll, W., *In situ* investigations of the electrodeposition and electrochromic properties of poly(3,4-ethylenedioxythiophene) ultrathin films by electrochemical-surface plasmon spectroscopy, *Langmuir*, **18**, 2002, 3555–3560.

[53] Lukosz, W., Tienfenthaler, K., Embossing techniwue for fabricating integrated optical components in hard organic waveguideing materials, *Opt. Lett.*, **8**, 1983, 537–539.

[54] Chien, F.-C, Chen, S.-J, A sensitivity comparison of optical biosensors based on four different surface plasmon resonance modes, *Biosens. Bioelectron*, **20**, 2004, 633–642.

[55] Schasfoort, R. B. M., Tudos, J., *Handbook of surface plasmon resonance*, RSC Publishing, Cambridge, 2008.

[56] Neininger, G. G., Tobiska, P., Homola, J., Yee, S. S., Long-range surface plasmons for high-resolution surface plasmon resonance sensors, *Sens. Actuators B,* **74**, 2001, 145–151.

[57] Wark, A. W., Lee, H. J., Corn, R. M., Long-range surface plasmon resonance imaging for bioaffinity sensors, *Anal. Chem.*, **77**, 2005, 3904-3907.

[58] Huang, C. J.; Dostalek, J.; Knoll, W. Optimization of layer structure supporting long range surface plasmons for surface plasmon-enhanced fluorescence spectroscopy biosensors *J. Vac. Sci. Technol. B*, **28**, 2010, 66-72.

[59] Dostalek, J.; Kasry, A.; Knoll, W. Long range surface plasmons for observation of biomolecular binding events of metallic surfaces *Plasmonics*, **2**, 2007, 97-106.

[60] Huang, C. J.; Dostalek, J.; Sessitsch, A.; Knoll, W. Long-range surface plasmon-enhanced fluorescence spectroscopy biosensor for ultrasensitive detection of *E. coli* O157:H7., *Anal. Chem.*, **83**, 2011, 674-677.

[61] Sarid, D. Long-range surface-plasma waves on very thin metal-films *Phys. Rev. Lett.*, **47**, 1981, 1927-1931.

[62] Chabot, V., Miron, Y., Grandbois, M., Charette, P. G., Long range surface plasmon resonance for increased sensitivity in living cell biosensing through greater probing depth, *Sens. Actuators B*, **174**, 2012, 94-101.

[63] Kasry, A.; Knoll, W. Long range surface plasmon fluorescence spectroscopy *Appl. Phys. Lett.* **2006**, 89, 101106-1 -3.

[64] Berini, P., Long-range surface plasmon polaritions, *Adv. Opt. Photon.*, **1**, 2009, 484–588.

[65] Berini, P., Bulk and surface sensitivities of surface plasmon waveguides, *New J. Phys.*, **10**, 2008, 105010.

[66] Slavik, R.; Homola, J. Ultrahigh resolution long range surface plasmon-based sensor, *Sens. Actuators B.*, **23**, 2007, 10-12.

[67] Vala, M.; Etheridge, S.; Roach, J. A.; Homola, J. Long-range surface plasmons for sensitive detection of bacterial analytes, *Sens. Actuators B,* **139**, 2009, 59-63.

[68] Kasry, A.; Knoll, W. Long range surface plasmon fluorescence spectroscopy *Appl. Phys. Lett.*, **89**, 2006, 101106-1 -3.

[69] Y. Wang, W. Knoll, J. Dostalek, Bacterial pathogen surface plasmon resonance biosensor advanced by long range surface plasmons and magnetic nanoparticle assays, *Anal. Chem*., **84**, 2012, 8345-8350.

[70] Lindman, B., Dias, R., DNA interactions with polymers and surfactants, John Wiley, New Jersy, 2008.

[71] Dobrynin, A. V., Rubinstein, M., Theory of polyelectrolytes in the solutions and at surfaces, *Prog. Polym. Sci*., **30**, 2005, 1049 – 1118.

[72] Morga, M., Adamczyk, Z., Monolayers of cationic polyelectrolytes on mica-Electrokinetic studies, *J. Colloid Interface Sci*., **407**, 2013, 196 – 204.

[73] Lankalapalli, S., Kolapalli, V. R. M., Polyelectrolyte complexes: a review of their application in drug delivery technology, *Indian J. Pham. Sci*., **71**, 2009, 481 – 487.

[74] Chibowski, S., Grzadka, E., Patkowski, J., Comparison of the influence of a kind of electrolyte and its ionic strength on the adsorption and electrokinetic properties of the interface: Polyacrylic acid/MnO_2/electrolyte solution, *Colloids Surf., A*, **326**, 2008, 191 – 203.

[75] Molinari, R., Argurio, P., Poerio, T., Comparison of polyethylenimine, polyacrylic acid and poly(dimethylamine-co-epichlorohydrin-co-ethylenediamme) in Cu^{2+} removal from waste waters by polymer-assisted ultrafiltration, *Desalination*, **162**, 2004, 217 – 228.

[76] Xiao, S.; Shen, M.; Ma, H.; Guo, R.; Zhu, M.; Wang, S.; Shi, X. Fabrication of water-stable electrospun polyacrylic acid-based nanofibrous mats for removal of copper (II) ions in aqueous solution *J. Appl. Poly. Sci.* **2010**, *116*, 2409-2417.

[77] Mao, X.; Ding, B.; Wang, M.; Yin, Y. Self-assembly of phthalocyanine and polyacrylic acid composite multilayers on cellulose nanofibers *Carbohydr. Polym.* **2010**, *80*,839-844.

[78] Fery, A., Scholer, B., Cassagneau, T., Caruso, F., nanoporous thin films formed by salt-induced structural changes in multilayers of poly(acrylic acid) and poly(allylamine), *Langmiur*, **17**, 2001, 3779 – 3783.

[79] A. Urrutia, J. Goicoechea, P. J. Rivero, I. R. Matias, F. J. Arregui, Electrospun nanofiber mats for evanescent optical fiber sensors, *Sens. Actuators B*, **176** 2013, 569-576.

[80] L. Xiong, T. Yang, Y. Yang, C. Xu, F. Li, Long-term in vivo biodistribution imaging and toxicity of polyacrylic acid-coated upconversion nanophosphors, *Biomaterials*, **31**, 2010, 7078-7085.

[81] R. Zugle, T. Nyokong, Electrospun polyacrylic acid polymer fibers functionalized with metallophthalocyanines for photosensitizing and gas sensing applications, *J. Macromol. Sci. A.*, **49**, 2012, 279-287.

[82] Ding, B.; Yamazaki, M.; Shiratori, S. Electrospun fibrous polyacrylic acid membrane based gas sensors *Sens. Actuators B,* **106**, 2005, 477-483.

[83] Ding, B.; Kim, J.; Miyazaki, Y.; Shiratori, S. Electrospun nanofibrous membranes coated quartz crystal microbalance as gas sensor for NH_3 detection *Sens. Actuators B,* **101**, 2004, 373-380.

[84] Lee, S. W., Takahara, N., Korposh, S., Yang, D. H., Toko, K., Kunitake, T., Nanoassembled thin film gas sensors. III. Sensitive detection of amine odors using TiO_2/poly(acrylic acid) ultrathin film quartz crystal microbalance sensors, *Anal. Chem*. **82**, 2010, 2228 – 2236.

[85] Akkahat, P.; Hoven., V.P. Introducing surface-tethered poly(acrylic acid) brushes as 3D, *Colloids Surf., B* **2011**, *86*, 198-205.

[86] Pyun, J.C.; Beutel, H.; Meyer, J,-U.; Ruf, H.H. Development of a biosensor for E.coli based on a flexural plate wave (FPW) transducer, *Biosens. Bioelectron*. **1998**, *13*, 839-845.

[87] Kutyla, M. J., Boehm, M. W., Strokes, J. R., Shaw, P. N., Davies, N. M., McGeary, R. P., Tuke, J., Ross, B. P., Cyclodextrin-crosslinked poly(acrylic acid): adhesion and controlled release of Diflunisal and fluconazole from solid dosage forms, *APPS Pharm. Sci. Tech*., **14**, 2013, 301-11.

[88] Kutyla, M. J., Lambert, L. K., Davies, N. M., McGeary, R. P., Shaw, P. N., Ross, B. P., Cyclodextrin-crosslinked poly(acrylic acid): Synthesis, physicochemical characterization and controlled release of Diflunisal and Fluconazole from hydrogels, *Int. J. Pharm.*, **444**, 2013, 175 – 184.

[89] Lonklin, J, Shinbo, K., Onishi, K., Kaneko, F., Bao, Z., Advinvula, R. C., Ambipolar organic thin film transistor-like behavior of cationic and anionic phthalocyanines fabricated using layer-by-layer deposition form aqueous solution., *Chem. Mater*., **15**, 2003, 1404 – 1412.

[90] Decher, G., Hong, J. D., Buildup of ultrathin multilayer films by a self assemble process: I. Consecutive adsorption of anionic and cationic bipolar amphiphiles, *Makromol. Chem., Macromol. Symp*., **46**, 1991, 321 – 327.

[91] Decher, G., Hong, J. D., Schmitt, J., Buildup of ultrathin multilayer films by a self-assembly process: III. Consecutively alternating adsorption of anionic and cationic polyelectrolytes on charged surfaces, *Thin Solid Films*, **210**, 1992, 831 – 835.

[92] Decher, G., Fuzzy nanoassemblies: Toward layered polymeric multicomposites, *Science*, **277**, 1997, 1232 – 1237.

[93] Zhai, L., McCullough, R. D., Layer-by-layer assemble of polythiophenes, *Adv. Mater*., **14**, 2002, 901 – 905.

[94] Fendler, J. H., Self-assembled nanostructured materials, *Chem. Mater*., **8**, 1996, 1616 – 1624.

[95] Baba, A., Park, M. –K., Advincula, R. C., Knoll, W., Simultaneous surface plasmon optical and electrochemical investigation of layer-by-layer self-assembled conducting ultrathin polymer films, *Langmuir*, **18**, 2002, 4648 -4652.

[96] Park, M. –K., Deng, S., Advincula, R. C., pH-sensitive biopolar ion-permselective ultrathin films, *J. Am. Chem. Soc*., **126**, 2004, 13723 – 13731.

[97] A. Baba, P. Taranekar, R. R. Ponnapati, W. Knoll, R. C. Advincula, Electrochemical surface plasmon resonance and waveguideenhanced glucose biosensing with N-Alkylaminated polypyrrole/glucose oxidase multilayers, *Appl. Mater. Interfaces*, **2**, 2010, 2347–2354.

[98] Sriwichai, S., Baba, A., Deng, S., Huang, C., Phanichphant, S., Advincula, R. C., Nanostructured ultrathin films of alternating sixthiophenes ans electropolymerizable polycarbazole precursor layers investigated by electrodhemical surface plasmon resonance spectroscopy, *Langmuir*, **24**, 2008, 9017 – 9023.

[99] Sathiyamoorthy, K., Murukeshan, V. M., Vijayan, C., Photoacoustic based surface plasmon resonance spectroscopy: an investigation, DOI:10.5772/52545.

[100] Zworykin, V. K., Hillier, J., Snyder, R. I., A scanning electron microscope, *ASTM Bull*., **117**, 1942, 15 – 23.

[101] Samerjai, T., Synthesis of platinum-loaded tungsten oxide nanoparticles and their applications, Ph.D., Dissertation, Chiang Mai University, 2013.

[102] Netsuwan, P., Mimiya, H., Baba, A., Sriwichai, S., Shinbo, K., Kato, K., Kaneko, F., Phanichphant, S., Long-Range Surface Plasmon Resonance Immunosensor based on Water-Stable Electrospun Poly(acrylic acid) Fibers, *Sens. Actuators B Chem*. **204**, 2014, 770–776.

[103] Chuekachang, S., Electrochemically controlled detection of some biomolecules on poly(2-aminobenzylamine) thin films by surface plasmon resonance spectroscopy, Ph.D. Dissertation, Chiang Mai University, 2013

CURRICULUM VITAE

Author's Name	Miss Paphawadee Netsuwan
Date of Birth	June, 28th, 1976
Place of Birth	Chiang Rai Province
Education Background	1999–2003 B.Sc. (Chemistry), Department of Chemistry, Faculty of Science, Chiang Mai University, Chiang Mai, Thailand
	2003–2005 M.Sc. (Chemistry), Department of Chemistry, Faculty of Science, Chiang Mai University, Thailand,
Scholarship	2011–2013 The Office of the Higher Education Commission, under the program Strategic Scholarships for Frontier Research Network, Thailand for the Ph.D.

Publications and Presentations

Journal Article

1. Netsuwan, P., Sriwichai, S., Phanichphant, S., Baba, A., Shinbo, K., Kato, K., Kaneko, F., Fabrication of Carboxylated Conducting polymer/CNTs Composites Thin Films for Immunosensor Application, Mol. Crys. Liq. Crys., 580, 2013, 7□14.

2. Netsuwan, P., Chaisu, W., Phanichphant, S., Sriwichai, S., Nanocomposite Thin Film of Poly(3-aminobenzoic acid) and Multiwalled Carbon Nanotubes Fabricated through Electrochemical Method, Adv. Mat. Sci. Eng., 2014, 6 pages, http://dx.doi.org/10.1155/2014/873028.

3. Netsuwan, P., Mimiya, H., Baba, A., Sriwichai, S., Shinbo, K., Kato, K., Kaneko, F., Phanichphant, S., Long-Range Surface Plasmon Resonance Immunosensor based on Water-Stable Electrospun Poly(acrylic acid) Fibers, Sens. Actuators B Chem. 204, 2014, 770–776.

Presentations

1. Netsuwan, P., Sriwichai, S., Panichphant, S., Baba, A., Shinbo, K., Kato, K., Kaneko, F., Electropolymerization of Carboxylated Conducting Polymer/CNTs composites for use as Immunosensor, Oral Presentation, International Symposium on Electrical Insulating Materials (ISEIM 2011), 6−11 September 2011, The Center of Conventional Singapore, Kyoto, Japan.

2. Netsuwan, P., Sriwichai, S., Phanichphant, S., Baba, A., Shinbo, K., Kato, K., Kaneko, F., In situ Electrochemical-surface Plasmon Resonance Spectroscopy for studying Polybenzothiophene Derivatives/CNTs Composited Films, Poster Presentation, The 6th International Conference on Technological Advances of Thin Films & Surface Coatings, 14−17 July 2012, Singapore Management University, Singapore.

3. Netsuwan, P., Sriwichai, S., Phanichphant, S., Baba, A., Shinbo, K., Kato, K., Kaneko, F., Fabrication of Carboxylated Conducting polymer/CNTs

Composites Thin Films for Immunosensor Application, Poster Presentation, KJF International Conference on Organic Materials for Electronics and Photonics, (KJF 2012), 29 August −1 September 2012, Tohoku University, Sendai, Miyagi, Japan.

4. Netsuwan, P., Baba, A., Sriwichai, S., Shinbo, K., Kato, K., Kaneko, F., Panichphant, S., Long-Range Surface Plasmon Resonance Biosensor based on Water-Stable Electrospun Poly(acrylic acid) Fibers, Oral Presentation, IEEJ, 21 – 23 March 2012, Hiroshima, Japan.

5. Netsuwan, P., Baba, A., Sriwichai, S., Shinbo, K., Kato, K., Kaneko, F., Panichphant, S., Fabrication of Water-Satble Electrospun Poly(acrylic acid) Fibers for Long-Range Surface Plasmon Resonance Biosensor, 18–19 November 2011, Kanazawa, Japan.

Working experience	2004-Present Lecturer of Chemistry, Faculty of Science and Agricultural Technology, Rajamangala University of Technology Lanna, Chiang Rai, Thailand,